Journal of Marine Research, 63, 227–261, 2005

Intense short-period internal waves in the ocean

by Konstantin Sabinin[1] and Andrey Serebryany[2]

ABSTRACT

Trains of quasi-periodic high-frequency internal waves (IWs) of large amplitude are common in the upper thermocline of the ocean. Sources for these waves may be different ones but it is not always possible to experimentally establish them for certain. We analyzed results of many IW experiments carried out in different representative regions of the World Ocean, including continental margins in the Mid-Atlantic Bight, in the northwestern Pacific at Kamchatka, the Seyshelles-Mascarene bottom rise, and some regions of the open ocean where the intense short-period IWs occur. Comparative analysis of the intense IWs observed in the Mid-Atlantic Bight and at Kamchatka revealed similarity and difference in the IW field in these regions differing by their bottom topography. Most of the observed trains in the Mid-Atlantic Bight propagate shoreward from the shelf break in the form of soliton packets or solibores and do not occur seaward from the shelf. The soliton trains in the northwestern Pacific at Kamchatka are common not only at the shelf edge but also in deep water where they propagate in various directions that seem to be related to the supercritical steepness and complicated form of the continental slope. Observation of generation and evolution of the IW trains at the Seyshelles-Mascarene bottom rise where huge internal solitons have been encountered has shown that the undular bore generated at the lee side of the bottom rise gradually evolves in a train of solitons with the trailing linear waves. Large solitons are generated also in deep water as a result of ray propagation of the internal tide emanated from the rise as happens in the Bay of Biscay. Certain consequences of the IW interaction with the background current leading to intensification of the high-frequency waves were observed in several regions of the open ocean. Revealed dependency of the intense wave propagation direction on the current direction, and closeness of the wave frequency to the frequency at which the waveguide steeply tapers may be regarded as clear evidences for the important role which currents play in the IW intensification.

1. Introduction

As was clearly shown by Fofonoff (Fofonoff, 1969) as early as 1969, oscillations of the thermocline from the inertial (f) to the buoyancy (N) frequencies are nearly fully governed by internal waves (IWs). In the open ocean, the spectrum of these waves can be satisfactorily described by the universal model of Garrett-Munk (Garrett and Munk, 1975) for nearly all frequencies except for three particular bands: the inertial, tidal, and high-frequency. In these bands, peaks of the spectral density exist in the background spectra of currents (which decay in frequency) and in the vertical oscillations of the

1. N. N. Andreyev Acoustics Institute, Moscow, 117036, Russia. ***email: ksabinin@akin.ru***
2. N. N. Andreyev Acoustics Institute, Moscow, 117036, Russia. ***email: serebryany@akin.ru***

thermocline. The lowest frequency peak, slightly higher than the local f, is caused by intermittent inertial oscillations accompanying moving atmospheric and oceanic fronts, upwelling phenomena, transient sea currents and so on. The peaks at the diurnal and semidiurnal periods are caused by internal tides that are generated in the interaction between tidal currents and bottom relief.

The high-frequency peaks near N are associated with the sporadic occurrence of trains of short-period IWs with large amplitudes which are especially pronounced in the upper thermocline of the ocean. In contrast to background oscillations that are more or less stationary, isotropic, and multimode, the short-period IWs are anisotropic, transient, inhomogeneous in space, and low mode in structure (Sabinin, 1973; Brekhovskikh *et al.,* 1975; Konyaev and Sabinin, 1992). Because of their high space-time intermittence and variability, these waves are not always apparent in averaged spectra: they produce weakly pronounced peaks and plateaus in the spectral curve. In some cases, their amplitudes can be very high. These high amplitude waves cause sharp space-time variability of the oceanographic fields and currents. That is why studies of these phenomena are urgent for underwater navigation, ocean acoustics, marine trade, and underwater engineering activities. As a rule, the short-period IWs are strongly nonlinear, and play an important role in diapycnal mixing of sea waters.

Short-period IWs are insufficiently studied. Although their most pronounced manifestations, the solitons near continental edges, have been observed in many experiments (Jackson and Apel, 2002), the origin of intense short-period IWs that occur in the open ocean is not fully understood.

In this paper we analyze numerous experimental data on IWs obtained in different regions of the Atlantic, Indian, and Pacific oceans, the ample data of the JUSREX (Joint US/Russia Internal Wave Remote Sensing Experiment, 1992) (Gasparovic and Etkin, 1994) and SWARM (Shallow-Water Internal Wave Acoustic Scattering Experiment, 1995) (Apel *et al.,* 1997) experiments on the Mid-Atlantic Bight shelf, and some unpublished results to characterize the structure and the origin of intense short-period IWs for different oceanic environments. In this analysis, the term "intense" refers to IWs in which the following conditions are simultaneously met: the amplitude of vertical displacements (a) are about 5 m or more, the amplitude of orbital velocities (U) are about 5 cm/s or more, and the nonlinear parameter $n = U/C = da/dz \geq 0.1$, where C is the phase speed of the waves, and z is the depth. (Nonlinear parameter as large as 3.0 was reported, for instance, in Stanton and Ostrovsky (1998).) Such conditions are approximately satisfied for typical short-period IWs that propagate with a phase speed of about 0.5–1 m/s, in the form of trains of intense oscillations in the upper thermocline of the ocean. The periods of such waves are usually equal to several tens of minutes, the wavelengths are several hundreds of meters. The choice of the aforementioned criteria is determined by the fact that the waves with such parameters produce noticeable time-space variability in current field and oceanographic characteristics. This variability is an important factor in practical applications and in the process of water mixing.

In Section 2, the waves at shelf edges are described. This section consists of two parts in which the internal solitons on the USA Atlantic coast (2a) and on the coast of the Kamchatka Peninsula (2b) are considered. Two parts of Section 3 analyze the intense IWs of the open ocean: those existing near bottom rises (3a) and in the regions where the waves are enhanced by interaction with low-frequency (background) currents (3b).

2. Waves at shelf edges

As typical examples, we consider IWs in two regions that strongly differ in their hydrographic conditions, namely, the waves on the broad shelf of the USA Atlantic coast and on the narrow shelf and the continental slope of Kamchatka. The latter shelf transitions to the deep Kuril-Kamchatka Trench and has steep and complex relief, with large underwater hills (in addition to the canyons that are characteristic for ordinary continental slopes). Near the shelf edge, the strong Kamchatka current exists, with meanders and eddies that significantly influence the structure of the IWs.

a. Waves at the Mid-Atlantic Bight Shelf

In summer, high-intensity short-period IWs nearly always exist over the relatively flat shelf of the USA Atlantic coast. These IWs propagate from the shelf break toward the coast, either as trains of internal solitons or as undular bores or "solibores" (Apel *et al.,* 1997; Apel, 2003). Intensive studies of the solitons, which seem to have started here earlier than anywhere else, were mainly based on analyzing the surface manifestations of the IWs (see, for instance, Apel *et al.,* 1975). However, there also exists a large number of *in-situ* measurements of the internal solitons. The measurements show that the amplitudes of vertical displacements sometimes exceed 10 m in this region, and the velocities of orbital currents reach several tens of cm/s.

The objective of our paper is far from trying to review all the publications on solitons in this region. However, we note the works of Liu (1988), Apel *et al.* (1998), Gasparovic *et al.* (1988), and Colosi *et al.* (2001), which studied internal solitons and their evolution at the shelf, and the CD Atlas (Jackson and Apel, 2002), which generalizes observations of surface traces of the solitons. The solitons emerge over the shelf, near the break, and, in the form of several waves with long crests oriented mainly along the isobaths, propagate toward the coast. The distance between the crests varies from 0.3 to 1.2 km, with a mean value of 0.6 km, while the mean distance between the wave trains is 17.5 km, which is close to the wavelength of the semidiurnal internal tide of the first mode.

The origin of the solitons is usually attributed to two mechanisms. The first involves the nonlinear evolution and disintegration of the internal tide as it propagates from the generation point at the shelf break (internal tide mechanism). The second is the decomposition of internal hydraulic jumps generated off the shelf break by an offshore flow, usually provided by the ebbing barotropic tide (lee-wave mechanism (Apel *et al.,* 1998)).

To characterize soliton-like internal waves at the ocean shelf in more detail, let us

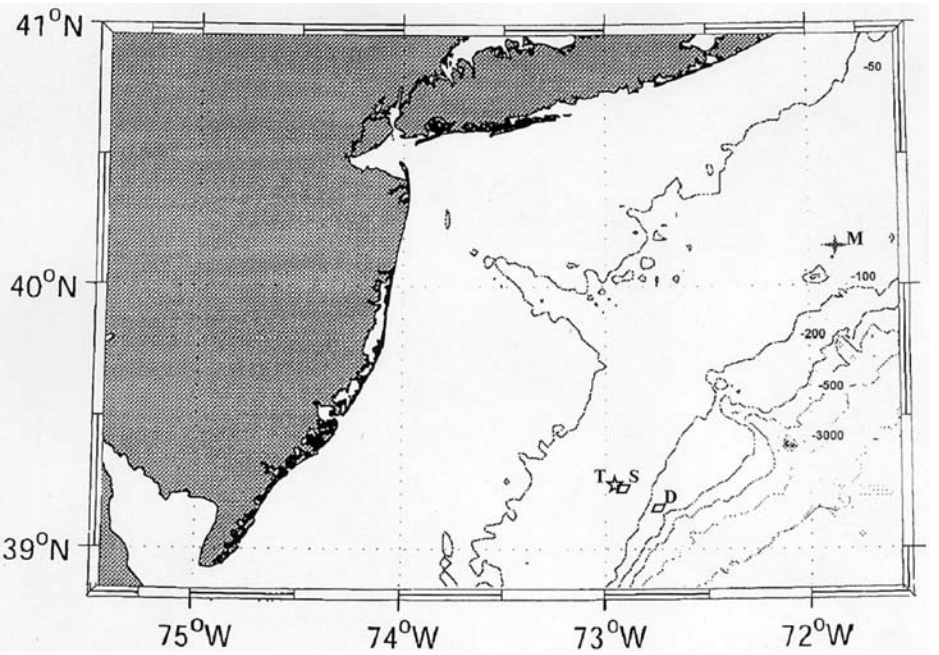

Figure 1. Location of JUSREX moorings 3 (M), and SWARM thermistor strings (T), Shallow-Site (S) and Deep-Site (D) ADCPs.

consider some results of the JUSREX and SWARM experiments. In these experiments, IWs were thoroughly measured in the Mid-Atlantic Bight in July, 1992 and July and August, 1995, respectively. Figure 1 shows the layout of the experiments whose data are to be discussed here.

In the SWARM experiment, at the end of July, 1995, an array of three closely spaced thermistor strings was used. With this instrument, a classical train of three rank-ordered internal solitons was observed that propagated toward the coast with the velocities from 0.8 to 0.6 m/s and amplitudes from 12 to 4 m (Julian date (JD) 211, (Apel *et al.,* 1997)). This train is well pronounced in Figure 2a, the data JD 210.95 to JD 211.05. In the second part of the record, the trains are also noticeable but their structure differs from the classical one, and the wave amplitudes are a factor of about two lower than in the first train. It is worth mentioning that, in both cases, the consecutive trains appeared after a quarter rather than a half day.

Figure 3 shows some results of currents measured in the SWARM experiment. The currents were measured at two separate locations, 16.5 km apart, referred to as the "Shallow-Site" (hereafter, "S") and "Deep-Site" (hereafter, "D"), using ADCPs that were moored 4 m above the sea floor, facing upward. D was placed in 103 m of water near the shelf break, and S was in 75 m of water (see Fig. 1). Measurements at S were collected in

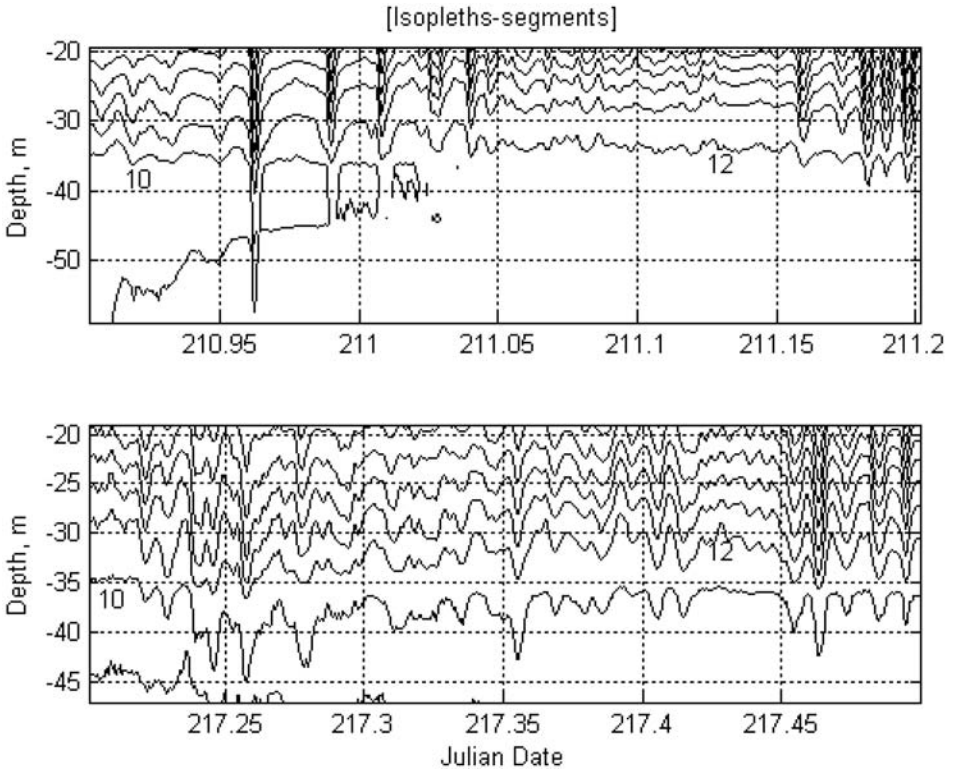

Figure 2. Isotherms for two segments of the SWARM thermistor string #598 record. (Isotherms are given for even degrees from 8 to 24°C.)

16 4-m-depth bins centered from 67 to 7 m in depth. The data at D were recorded in 22 depth bins centered from 95 to 11 m. The baroclinic component of the current is examined by removing the depth-averaged current and high-pass filtering the data (cutoff frequencies ~0.3 cph). The baroclinic currents are used to describe the solitons. Figures 3b and 3c show absolute values and vectors of the currents in the trains of strong solitons that were observed at D (the first half of the record, Fig. 3c) and at S (the end of the record, Fig. 3b). One can notice that, in both cases, the solitons propagated toward the coast, and their amplitudes became somewhat lower at the end of the record. Figure 3d presents the vectors of barotropic (averaged in vertical) low-frequency (lower than 0.03 cph) currents at the shelf break. Apel *et al.* (1997) attribute the pronounced attenuation of the solitons near D to the enhancing of the currents after JD 214. (It can be seen also in the lower trace in Fig. 3a, where there are fewer spikes after day 214.) According to Apel *et al.* (1997), this suggests that the mechanism of soliton generation is more consistent with lee-waves rather than with internal-tide nonlinear evolution.

However, such contradistinction of the two hypotheses is hardly worthwhile because the

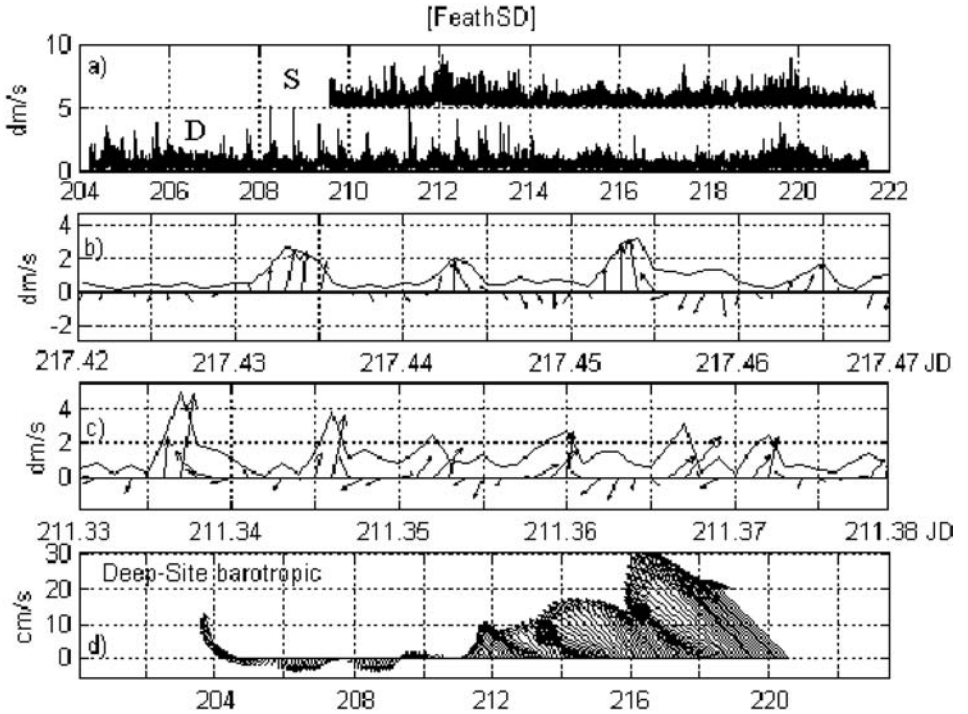

Figure 3. Upper layer soliton currents ($F > 0.3$ cph) at the Shallow (S) (a, b), and Deep (D) sites (c), and low-frequency ($F < 0.03$ cph) barotropic currents at D (d). (a) Current magnitude at D and S (shifted by 5 dm/s) upon time shown in Julian days. (b–c) Current vectors and magnitude at S (b) and D (c) for different segments. Upward direction of the arrow is due 306°T (up slope).

two mechanisms are physically identical. Actually, the nonlinear disintegration of the steep internal front takes place in both cases. Such disintegration happens either at the back side of internal tidal wave propagating in the near-surface pycnocline, or in the hydraulic jump off the shelf break. Certain accumulation of the nonlinear effects is necessary for the disintegration of the initial wave, thus some critical path length (or propagation time) is required. With a strong head current, the wave passes the critical distance relative to the water in less time, even if the wave remains fixed relative to the bottom (as in the case of lee waves). Hence, the disintegration of the wave into solitons begins earlier than in the case of propagation and evolution of the internal tide in stationary water or down current.

In view of the aforementioned statements, one expects that the trains of solitons appear earlier (later) for stronger seaward (shoreward) flow. Just this phenomenon can explain the appearance of the solitons at point S, which is closer to the coast (Fig. 3b) and at the thermistor string T (Fig. 2), after the enhancing of the shoreward flow in 214 JD. The trains observed near S (217 JD) did not appear near D (16.5 km closer to the shelf break). These waves differ from the trains observed earlier (211 JD) in that they have lower amplitudes,

shorter time intervals between the adjacent solitons, and a structure close to that of a solibore (see Fig. 2). The aforementioned facts indicate the younger age of the later train. Hence, the experimental data agree with the assumption that these solitons are created in the evolving internal tidal wave; the stronger the head flow, the closer the point of disintegration from the wave source (shelf break). Note the rather strong train of solitons at D appears at the end of the record when the shoreward flow reaches its maximum. One may conclude that the soliton appearance at D is determined not only by the background currents but also by variation of the density stratification at the shelf edge.

Let us now consider the important issue of the periodicity of appearance of the solitons at the shelf. This periodicity is commonly assumed to be close to semidiurnal frequency because the semidiurnal tides are considered to be the main source for the soliton trains. Figure 4 shows time variations in the energy of the soliton currents measured in the SWARM and JUSREX experiments. The energy was estimated as an integral of the running spectrum of the currents within the frequency band 1 to 15 cph, over the intervals 3.2 (in SWARM) and 2.5 hrs (in JUSREX) that overlapped by 3/4 of their lengths, with the shifts 0.8 and 0.6 hrs, respectively. Figure 4a presents the energy of the horizontal currents at D and S, in the upper layer. Figure 4b shows the energy of the vertical currents at JUSREX mooring M (see Fig. 1), as measured by the UCM40 Mk II three-axis current meters in the pycnocline, at 29 m. The semidiurnal periodicity in the soliton energy variation is noticeable only for D; it manifests itself in the form of a pronounced peak in the spectrum at 2 cpd (Fig. 4c). In the spectrum S, there is no semidiurnal peak at all. In addition to the semidiurnal peak, the JUSREX spectrum (Fig. 4d) has peaks at the inertial frequency (1.3 cpd), and at 3 and 4.1 cpd. The 4.1-cpd peak corresponds to the first harmonic of tidal oscillations. The appearance of this harmonic is quite expected in view of the nonlinearity of the internal tide that generates solitons. The 3-cpd peak can be considered as a consequence of the nonlinear interaction between the tidal and inertial oscillations (see Davies and Xing, 2003). The peak at 1.3 cpd, indicates a significant contribution of inertial waves in the generation of the trains of internal solitons in this region.

Generally, the spectrum of currents measured in the JUSREX experiment is dominated by the inertial rather than tidal oscillations because of the strong variability in winds. Rapid (in 1–2 days) changes in wind speeds, up to 10–15 and even 20 m/s (in the morning, July 15) were observed. These variations were accompanied by a rotation of wind direction, mainly clockwise, from east to southwest and west. As a whole, southwest winds dominated during the experiment, i.e. winds that are favorable for upwelling at the inner shelf. Offshore of the upwelling front (that is, at the outer shelf), a zone of negative vorticity in the current field should be originated, as was reported in Chant (2001). In this zone, inertial waves can propagate toward the coast; that is, in the direction of increasing planetary vorticity, and not only toward lower latitudes as is usually the case (Garrett, 2001). In view of these facts, the absence of the inertial component in the periodicity of the appearance of soliton trains (SWARM) can be related to the dominance of northwest

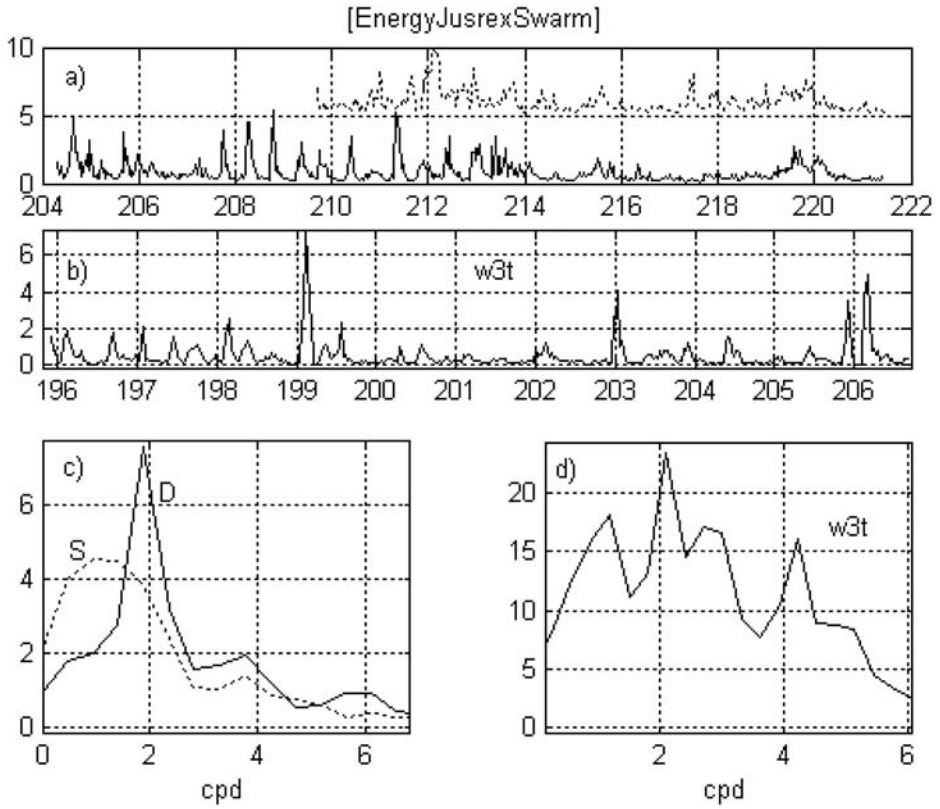

Figure 4. Variation of the soliton current energy in SWARM (a, c) and JUSREX (b, d). (a) Running spectral density (averaged in frequency band 1–15 cph) of the SWARM current magnitude in upper layer at D (11 m), and S (7 m, dotted) estimated in 3.2-hour segments shifted by 0.8 hours. (b) Running spectra of the JUSREX vertical currents at 29 m estimated in 2.5-hour segments shifted by 0.6 hours. (c, d) Spectra of records shown in (a) and (b), respectively. Vertical scales are in arbitrary units. Time is shown in (a, b) horizontal axis in 1995 (a) and 1992 (b) Julian dates.

downwelling winds (Apel *et al.,* 1997), which, in contrast to the upwelling winds in JUSREX, cannot lead to negative vorticity at the outer shelf.

The JUSREX-established importance of inertial oscillations on the generation of soliton trains is not the exception. Ivanov and Serebryany (1985; 1983) and Vlasenko *et al.* (1998), for instance, reported the appearance of trains with the inertial period (~17 hrs) in coastal zone of the Black Sea, where there are nearly no tides. Kim *et al.* (2001) observed generation of the soliton trains by inertial waves.

The structure of solitons in the JUSREX region was obscured by the closeness of the Hudson Canyon that created its own system of trains, which propagated along isobaths (Fig. 5), in contrast to more pronounced main trains propagating toward the coast. The

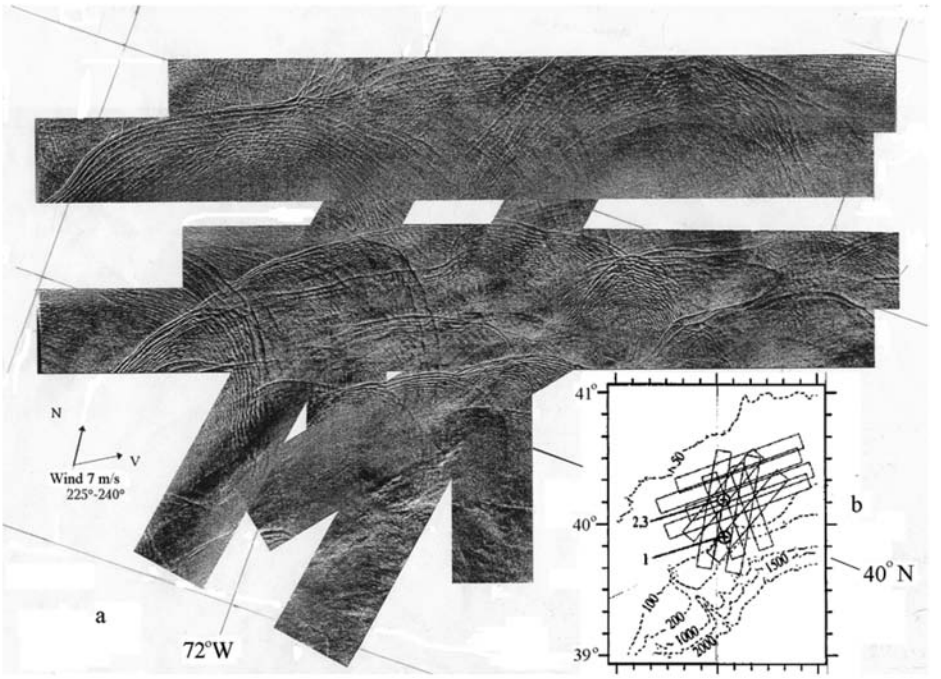

Figure 5. Radar imagery of internal waves in the New York Bight (JUSREX area) obtained by a superposition of airplane radar swaths along with a schematic representation of the surveyed area with location of moorings 1, 2, and 3 (x) and isobaths.

existence of this secondary system may also make the "time table" of the soliton arrivals more intricate.

An interesting feature of the shoreward-propagating trains is the closeness of the adjacent trains at the initial stage of their generation near the shelf break. The distances between the trains here were substantially shorter than the mean wavelength of the semidiurnal internal tide, this length being about 25 km (Vlasenko *et al.,* 1997). Zheng *et al.* (1993) observed similar phenomenon near the shelf break southwest of the Hudson Canyon and argue that two sources of solitons exist at the upper and lower parts of the continental slope (at the depths 160 and 1800 m, respectively). Without rejecting this explanation, one can also consider the Earth's rotation, which according to Lamb (1994), can lead to secondary depressions of the pycnocline that occur at the shelf break when the ebb-tide current changes to flood. This is a probable explanation for the aforementioned (Fig. 3) appearance of soliton trains at quarter-day rather than at half-day intervals.

To conclude, let us consider one more feature of the field of intense IWs in the Mid-Atlantic Bight. There is an absence of visible traces of the soliton trains at the ocean surface beyond the shelf. Actually, to our knowledge, there are no reports of such traces either in deep water or at the continental slope in this region, although the IW-caused

surface features are characteristic for many marginal regions of the ocean (e.g., the northeast Pacific (Lavrova and Sabinin, 1998), the Bay of Biscay (New and Pingree, 1992), and the North Brasilia shelf edge (Kuznetsov *et al.,* 1984). All these regions have steeper continental slopes than the Mid-Atlantic Bight. The insufficient steepness of the continental slope in the Mid-Atlantic Bight can be the cause of low intensity of the IWs propagating toward the ocean because the steeper the slope the higher the energy of the baroclinic tide radiated by the shelf edge to the open ocean (see Laurent *et al.* (2003) for instance). However, one can also look for an explanation in the specifics of the density stratification in the region at hand.

The main mechanism of IW surface manifestation is the modulation of surface waves by orbital currents in the IW. If these currents and their longitudinal gradients are strong enough, the IWs are visible at the surface, both in the optical and in the radar frequency bands. The surface traces allow one to estimate the spatial structure and, to some extent, the amplitude of the currents (Alpers, 1985); the latter being given by the expression: $U = C \cdot da/dz$. Because internal solitons propagate quickly and usually have large amplitude, they create pronounced surface traces, especially if the pycnocline is sharp and shallow, just as at the shelf of the Mid-Atlantic Bight. As the distance from the shelf edge increases, the pycnocline becomes weaker and deeper in this Atlantic region, and the near-surface orbital currents in IWs decrease. Moreover, such behavior of the pycnocline impedes the generation of internal solitons.

b. Internal waves at Kamchatka

The Pacific continental margin at Kamchatka drastically differs from that in the Mid-Atlantic Bight in the narrowness of the shelf, the steepness and complexity of the continental slope topography, and the existence of strong mean currents at the shelf edge. Internal wave trains propagating in different directions are common at the shelf edge and in deep water. The waves appear on the sea surface in typical form, with alternating bands of rough and smooth sea.

We present some results from long-term remote sensing experiments made in the northwestern Pacific by the Space Research Institute Russian Academy of Sciences (Etkin *et al.,* 1991). We focus on the summer seasons during 1977–1992. Radar images of internal waves at the sea surface were obtained by Russian Ku-band ($\lambda = 2.25$ cm) side-looking radar from a TU-134 aircraft laboratory. The radar swath of 12.5 km is illuminated on each side of the ground track, with a spatial resolution of about 25×25 meters. The spatial structure of the internal waves is a very complicated pattern composed of many soliton-like trains of various forms and propagation directions. We infer the propagation direction from radar images using the following criteria: the sea-surface reflectivity is enhanced at the leading front of the internal soliton which corresponds to a light strip on the radar image, and the wave lengths as well as the lengths of the soliton crests decrease from the leading to the rear part of a typical soliton train. On this basis, we determined the leading waves in the packets and the propagation direction. Wave front curvature does not seem to be a reliable

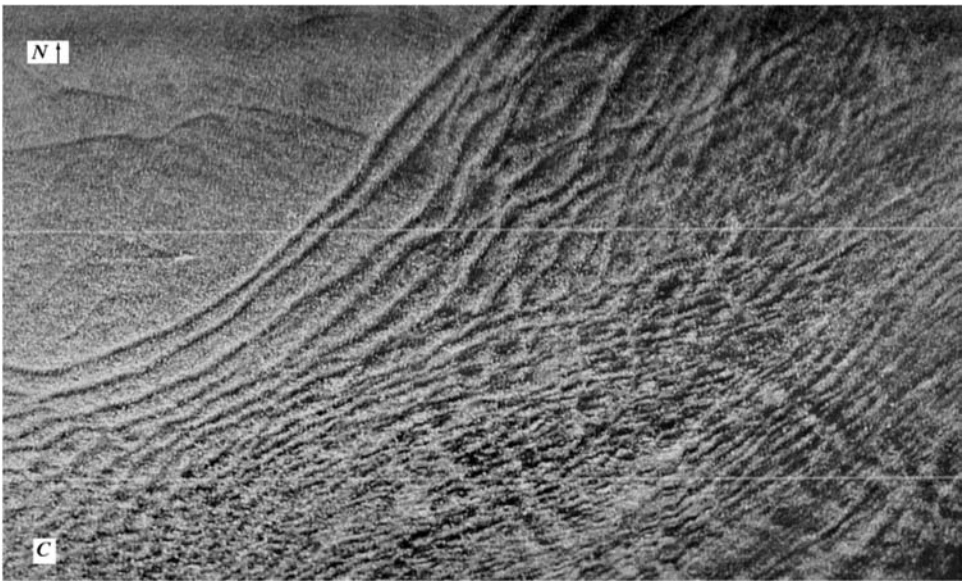

Figure 6. A radar image (24 · 12 km) of the IW manifestation (August 25, 1983). The train propagated shoreward from the deep water (see Fig. 7).

indicator for the propagation direction, although a convex curvature of IW fronts is typical for internal waves that are generated by localized sources. Interaction of the waves with sea currents can change the curvature. The impact of the current is apparently manifested in the curvature of the leading front of the IW packets (see Fig. 6).

Most of the trains were observed seaward from the shelf above the continental slope where internal wave surface manifestations frequently occur (Fig. 7). In contrast to the Mid Atlantic Bight, the observed surface patterns at Kamchatka usually are very complicated in character, indicating that different sources of IW's are found here at the shelf edge where underwater hills are common. Figure 8 illustrates a rather typical pattern of intersecting wave trains propagating in different directions. Notice the characteristic fractures of the intersecting wave fronts, which may be regarded as evidence of phase shifts caused by interacting solitons (see for instance, Apel *et al.* (1998)). Similar fractures can be found in nearly all radar images obtained from this region.

The existence of trains propagating to the open ocean may be connected with the supercritical steepness of the continental slope at Kamchatka, i.e. when the internal tide ray inclination $\gamma = \sqrt{(\omega^2 - f^2)/(N^2 - \omega^2)}$ at the bottom is less than the bottom steepness (here N, f and ω, are buoyancy, inertial and tidal frequencies, respectively). The internal tide radiates from the shelf break, reflects from the bottom offshore of the continental slope, and approaches the surface layer at some distance from the shelf edge. A similar pattern was observed in the Bay of Biscay (New and Pingree, 1990). The nonlinearity, n, of the internal tide increases in the upper ocean due to increasing buoyancy frequency N.

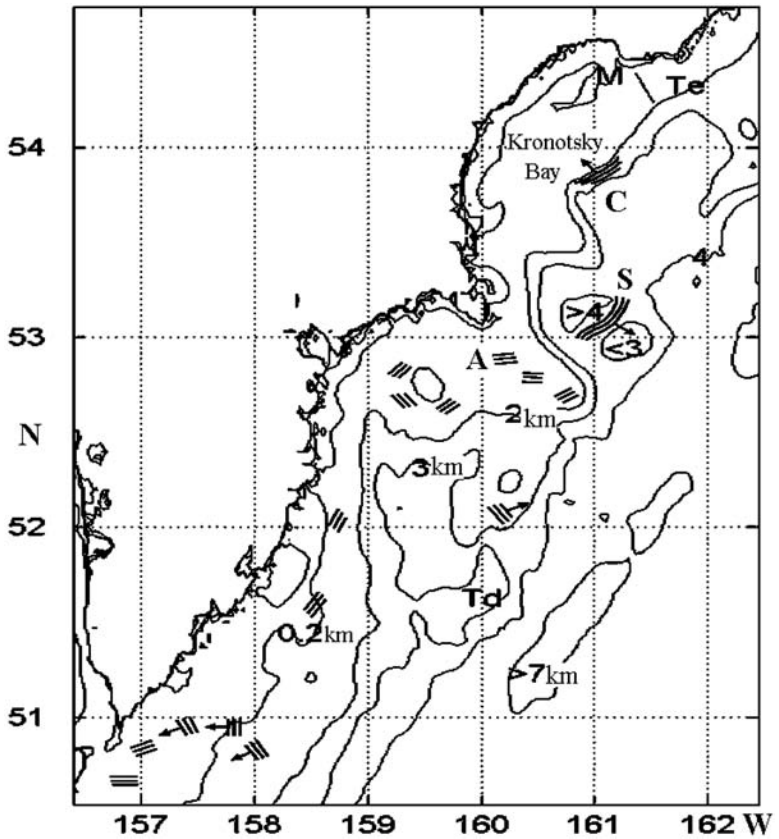

Figure 7. The Kamchatka test area showing regions where the surface manifestations of soliton trains have been observed. The wave crests are depicted schematically, the wave propagation directions (where they were unambiguous) are shown by arrows. Sites of the measurements made by moored sensor (M), and by sensors towed across the shelf edge (Te) and above deep water (Td) are depicted. Locations of the trains shown in Figures 6, 8 and 9 are denoted by C, A and S, respectively.

Indeed, $n(z) = a(z) \cdot k_z(z)$, where (in the frame of WKB approximation) $a(z) \sim N(z)^{-0.5}$, $k_z(z) \sim N(z)$, and $n \sim N^{0.5}$ (here $a(z)$ and $k(z)$ are the wave amplitude and vertical wavenumber, respectively with depth z defined in the WKB sense). Moreover, if the internal tide reflects at the bottom and rises in the wave propagation direction, then the amplitude, wavenumber and nonlinearity of the wave increase. Indeed, according to the internal wave reflection law $a_r/a_i = k_r/k_i = \cos(r - s)/\cos(r + s)$, where indexes i and r denote the incident and reflected waves, while γ and s are angles by which the bottom and the wavenumber are inclined to the horizontal plane, respectively. Therefore, the ratio of n for the reflected and incident waves is equal to $n_r/n_i = (\cos(r - s)/\cos(r + s))^2$. Such a situation apparently takes place in the Kronotsky Bay where the internal tide radiates from

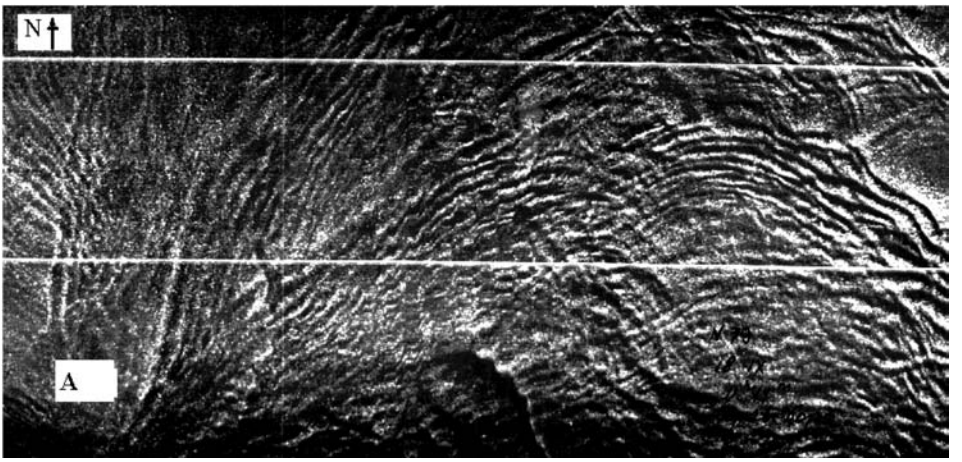

Figure 8. A radar image (24 · 12 km) showing the surface manifestations of internal waves at the shelf edge off Kamchatka (September 18, 1977).

the shelf break and reflects from the hill at the continental slope foot (Sabinin, 1996). It seems that a very characteristic train observed here is produced by the nonlinear disintegration of the internal tide reflected from the hill (Fig. 9). The rather unusual form of the wave fronts in this seaward propagating train suggests that wave refraction occurs at the meandering Kamchatka Current.

Besides remote sensing data we analyzed *in situ* measurements made during different expeditions at the shelf edge and deep water by moored and towed line sensors of temperature (Serebryany, 1996; 2000a), and by a towed thermistor chain. We used the line temperature sensors to avoid the fine structure contamination of temperature records obtained by point sensors. The line sensor (hereafter, LS) is an insulated vertical stretched wire of tens of meters in length. Its resistance changes in proportion to the average temperature of the layer over which it is stretched. The response of the line sensor to vertical displacements of the water layers is proportional to the vertical temperature gradient averaged over the length of the sensor, and it is more stable than the response of the point sensor. Such stability allows one to convert temperature data obtained by the line sensor into vertical displacement of the layer where the sensor is situated. We also used point sensors on the ends of the line sensor to measure the average temperature gradient (see Sabinin, 1982). For measuring the wave spatial structure, we used arrays consisting of three line sensors separated horizontally by several tens or hundreds of meters. (This type of array is described in detail by Brekhovskikh *et al.,* 1975.)

Eleven 10-km tow tracks were carried out in different directions in the vicinity of 52N, 160E. The thermocline elevation spectrum, averaged over 11 spectra for all tracks is plotted in Figure 10c. The Garrett-Munk towed spectrum (Garrett and Munk, 1975) is an order of magnitude weaker than the measured one.

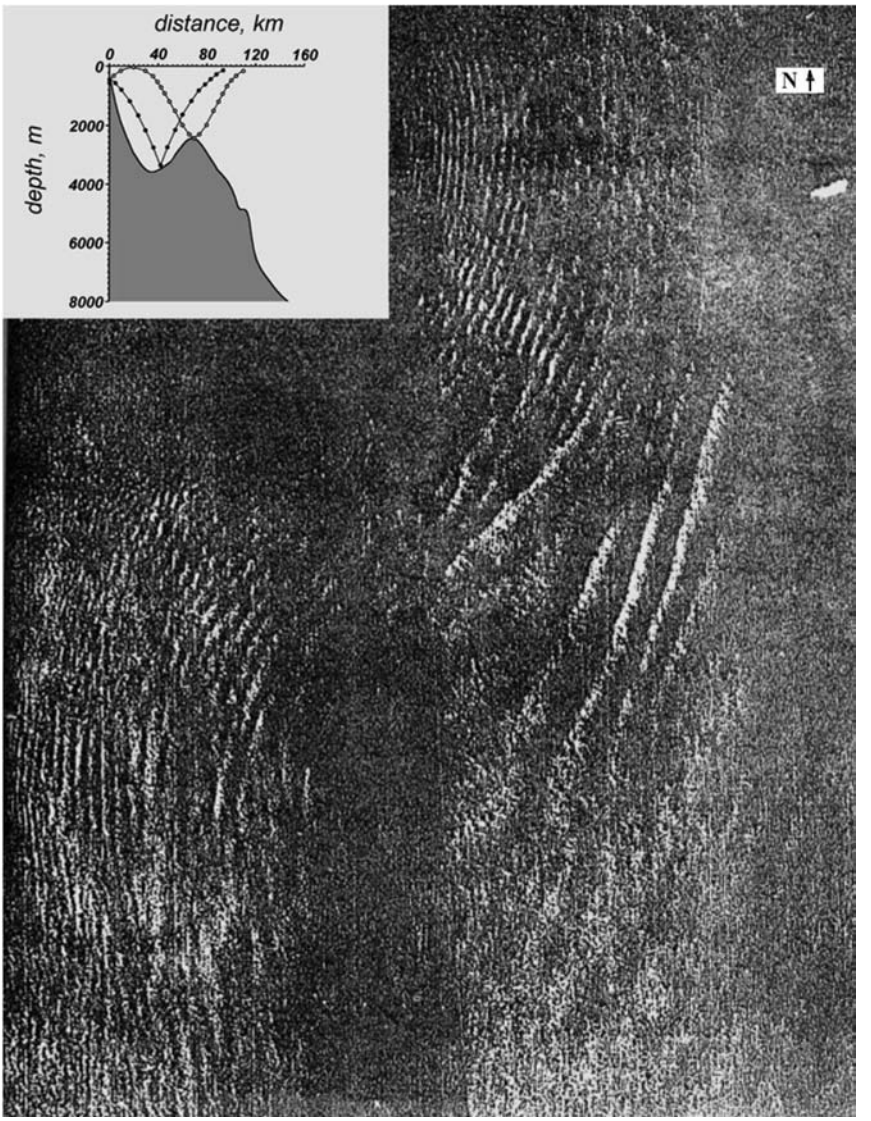

Figure 9. Radar image (28 · 43 km) of the internal wave surface manifestation above deep water off Kamchatka (September 8, 1981) (Etkin *et al.*, 1991). The internal tide rays emanated from the shelf break are shown in the inset together with the bottom profile.

Three soliton-like trains with heights up to 17 m can be seen in the line sensor record obtained from the vessel anchored on the shelf (Fig. 10a). The Garrett-Munk spectrum in the soliton frequency band (1–5 cph) is again significantly lower than the experimental spectrum (Fig. 10b). Most of our *in situ* observations included measurements of internal waves by the line sensors from anchored, drifting and towing vessels. In most cases,

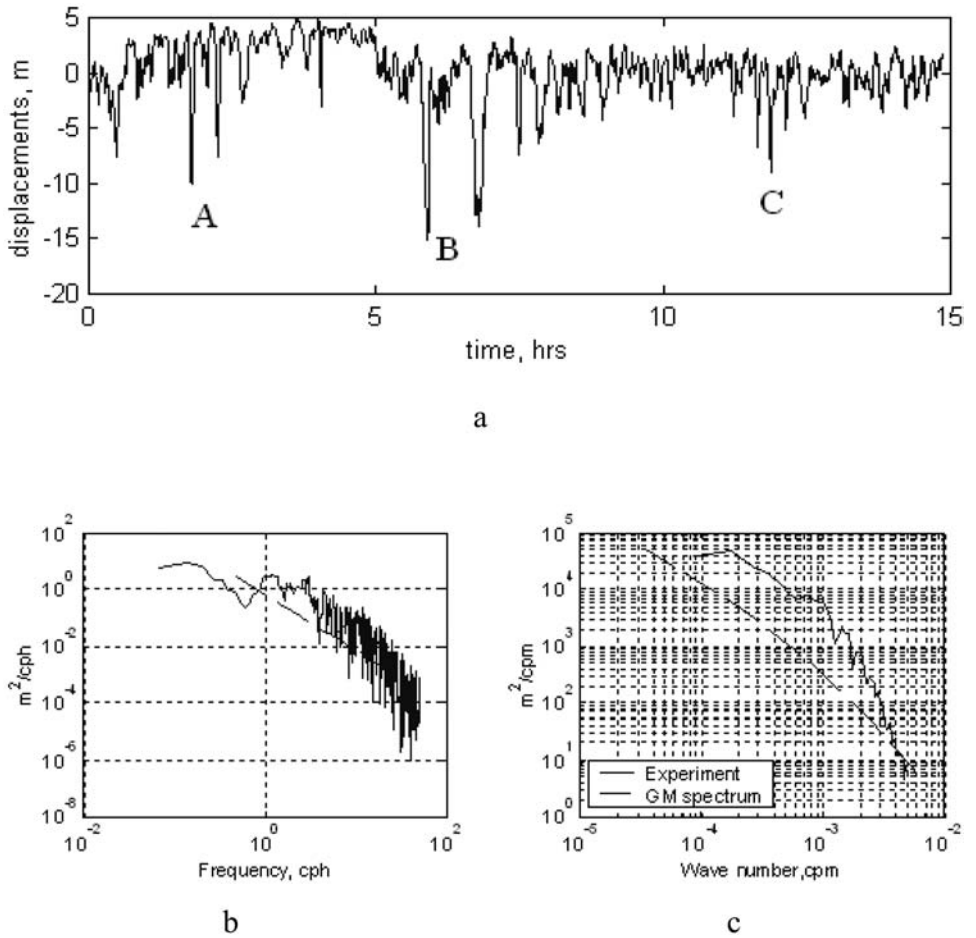

Figure 10. (a) Thermocline displacements measured by the moored line sensor on the Kamchatka shelf. (b) Spectrum of the record shown in (a). (c) Spectrum of the thermocline displacements measured by towed thermistor chain on eleven 10-km tracks of different directions above deep water. (site Td in Fig. 7). The Garrett-Munk spectrum is shown by dashed lines.

measurements from drifting and anchored vessels were made with spatial arrays. Such arrays enabled us to measure not only amplitudes and periods of internal waves but also the lengths and their propagation directions. In addition, we made yo-yo CTD soundings when intense internal waves passed. In several experiments, we also measured currents at different depths. The study area of our internal wave experiments covered nearly 400 km in the alongshelf direction.

As can be seen in Figure 11, two wave trains were encountered in the north part of the Kronotsky Bay in July 1990 at the ends of the 25-km tow across the shelf edge from deep water to the inner shelf (see Fig. 7). The deep-water train A evidently propagated to the

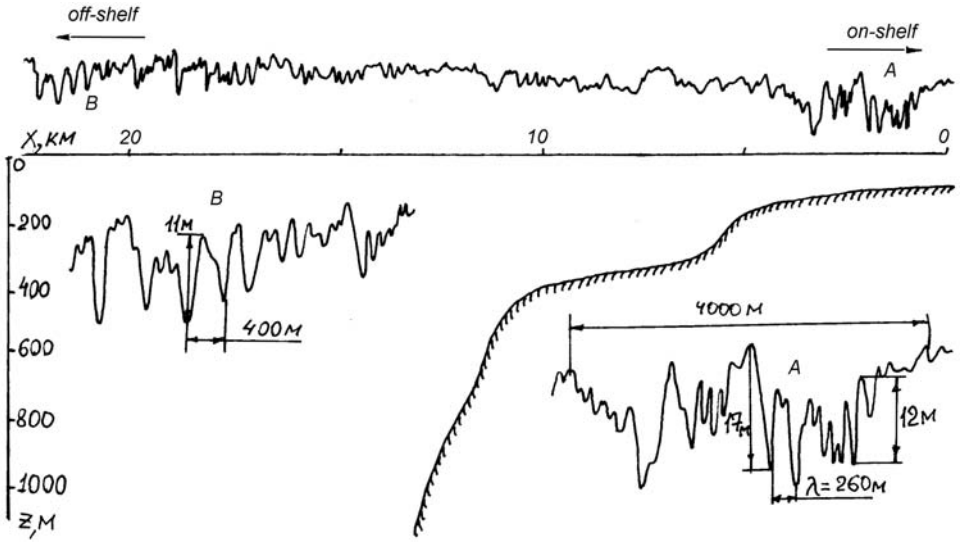

Figure 11. Thermocline displacements measured by the line sensor towed across the Kamchatka shelf edge.

open ocean while the shallow-water train B moved shoreward. Comparing the trains, we can see that internal waves in shallow water are narrower and higher than in deeper water. Both trains presumably are generated by the internal tide waves that radiate from the shelf break in different directions—to the shore and to the open ocean.

After the tow, the measurements were continued from the vessel anchored on the shelf. Three distinct soliton trains propagating to the shore were recorded by an array of three line sensors during 15 hours of measurements. The strongest train, consisting of four rank-ordered solitons of 18, 16, 11 and 8 m in height (train B in Fig. 10a), passed through the array 4.1 hours after train A and 6 hours earlier than train C. In contrast to trains A and B, the train C solitons were not rank-ordered and the highest 11-m soliton was in the middle of the train. The short time intervals between the trains suggests different locations of the wave sources, although all the trains seem to be generated by the evolving internal tide originating from the shelf break. The observed internal waves look like typical depression wave solitons (we compared their form with the soliton profile obtained from the Korteveg-de Vries equation), which are common for large-amplitude waves propagating on the thermocline close to the ocean surface.

Another important result was obtained during our observations in the south part of Kronotsky Bay (Serebryany, 2000b). This experiment consisted of two steps. In the beginning we made measurements of internal waves in the coastal zone from an anchored vessel. It was discovered that trains of internal waves were propagating shoreward. The research vessel then went seaward across the shelf, passing the shelf break and continental slope, and lay in drift over the deep water between the 2 and 3 km isobaths. During the drift

we carried out observations with the spatial antenna of line temperature sensors. Observations continued for almost 8 hours and the vessel was displaced 7.5 km to the south by the current (the weather was calm). During the drift we observed intense internal waves (heights up to 10 m) propagating to the east (seaward). Based on wave phase measured across three-element space antenna of line sensors, we estimated a phase speed of 0.34 m/s. Previously there were several airborne radar images (see for example Fig. 9) showing the surface manifestations of internal waves in this region. On the basis of these images it was assumed that internal waves emanate from the continental slope and propagate to the east (seaward) because bands connected with internal wave manifestations on the sea surface are wider in the eastern part of the image than in the western part. Our field observations of internal waves in the vicinity of the Kamchatka shelf edge have shown that there exist many sites at the shelf break and the continental slope where internal waves are generated and reflected.

The measurements of internal waves in the coastal zone of Kamchatka also captured the interesting phenomenon of solitary internal waves passing through "overturning point" on the shelf, with a transformation from depression to elevation waves (Serebryany and Pao, 2005).

We can summarize observational results on internal waves at Kamchatka as follows. Field observations show the existence of an intense internal wave field off the Pacific coast of Kamchatka. The main structural feature of the internal wave field is the simultaneous presence of two types of internal wave, those occurring on the shelf and propagating shoreward as trains of intense internal waves, and large amplitude internal waves that move seaward in deep water (continental slope and rise). The existence of solitary internal waves with typical amplitudes up to 10–15 m in the form of depression waves is a common phenomenon for both the shelf and the continental rise. The solitary waves exhibit properties of solitons. In particular, a dependence between amplitude and speed of the wave is observed.

3. Intense short-period internal waves in the open ocean

This section of the paper is devoted to the waves in representative regions of the World Ocean where the intense waves occur far from the coast. Very strong short-period waves are common in the western part of the Indian Ocean, especially in the area of the Seychelles-Mascarene bottom rise, where underwater sills between islands and shoals play the same role in the wave generation as the sills in straits (for instance, in the Gibraltar Strait, in the Sulu Sea straits (Apel *et al.,* 1985) etc. Results of the IW measurements in this region are discussed in Section 2.

Apparently different and yet unknown mechanisms act in creating the strong waves observed in open ocean basins. The deep Cape Verde Basin, where intense trains of short-period waves often occur far from significant bottom rises, seems to be a typical representative of such IW "hot spots" in the open ocean. Various dynamical processes (unstable fronts, inertial waves etc.) in the confluence zone of the Canary and North-

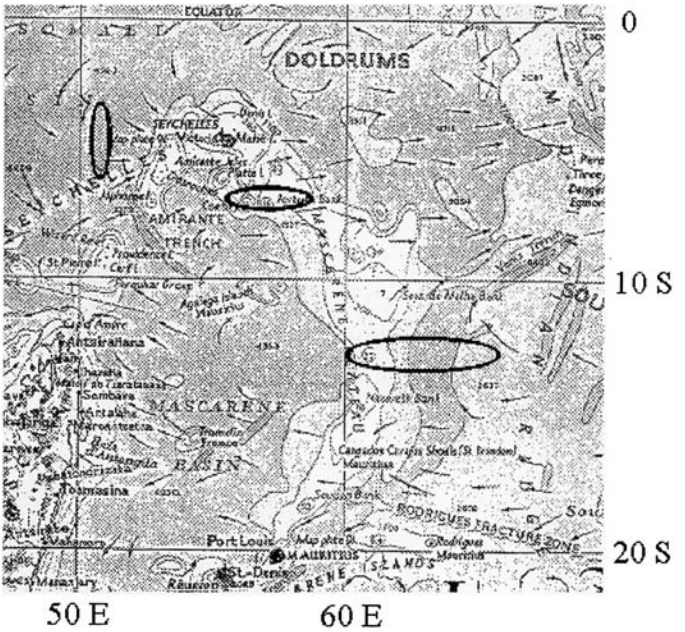

Figure 12. Location of the IW test areas (ellipses) in the Indian Ocean.

Equatorial currents may be responsible for the wave generation in this region. Typical parameters of the short-period waves and possible role of the background currents in the wave intensification in this and some other regions of the open ocean are discussed in part b of this section.

a. Waves at the Seyshelles-Mascarene bottom rise

The N.N. Andreyev Acoustics Institute (Moscow) performed several detailed IW experiments in the western part of the Indian Ocean (Brekhovskikh *et al.,* 1975; Sabinin, 1982; Sabinin *et al.,* 1987; Konyaev and Sabinin, 1992; Konyaev *et al.,* 1995). Most of the measurements were carried out in vicinity of the Seyshelles-Mascarene bottom rise (Fig. 12).

The IW observations were carried out by using: (a) towed and drifting arrays of line sensors (LS) in the upper thermocline; (b) measurements from a drifting ship via "yo-yo" CTD casts and vertical chains of line temperature sensors; (c) sequenced photographs of the sea-surface manifestations of IWs on a radar screen; (d) echo sounder recordings of sound scattering layers. The configuration of the LS arrays resembled the one shown in Figure 19, although the number and the spacing of the line sensor's used in different experiments varied. The spatial structure of the waves encountered and their propagation speeds were also estimated by using radar images of the wave surface manifestations. The latter were very strong there: long bands of calm

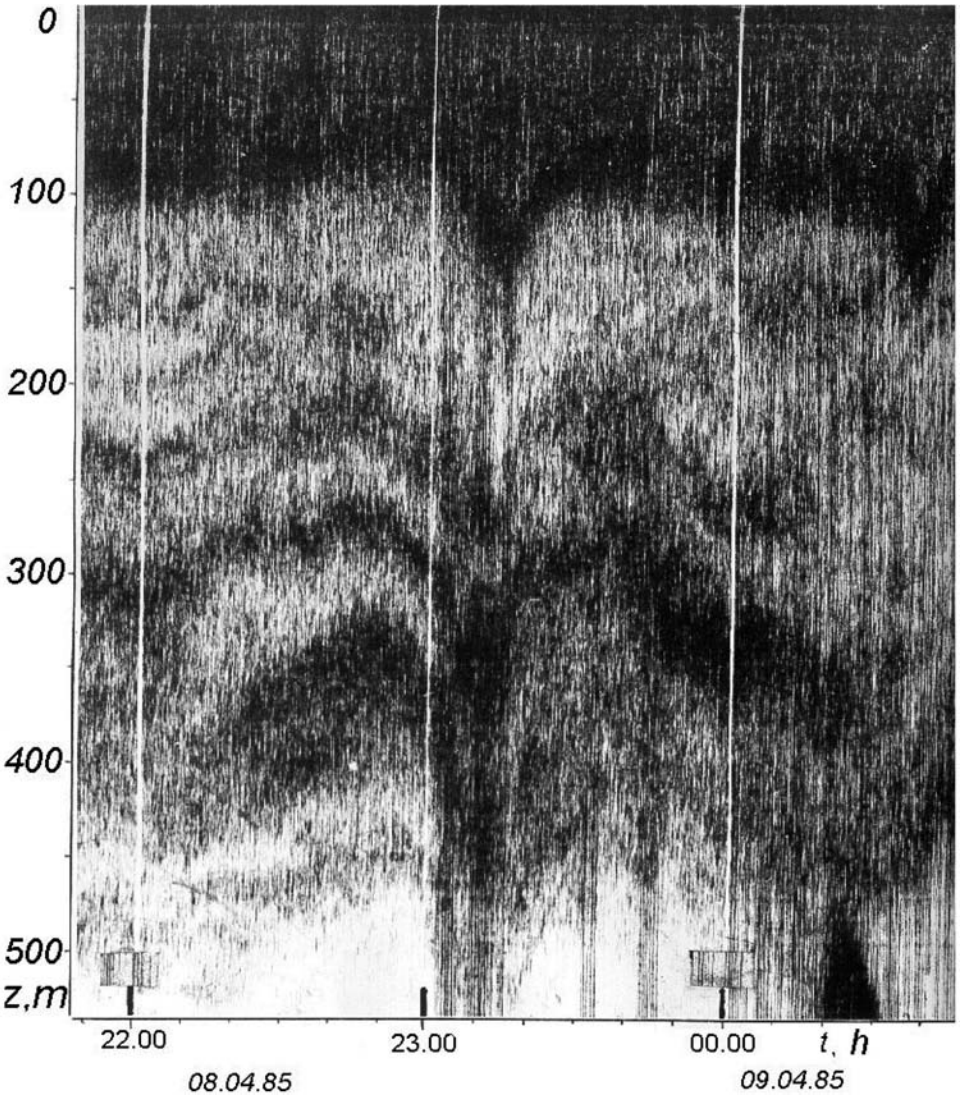

Figure 13. Record of the sound scattering layers obtained from the R/V drifting within the Seyshelles Archipelago in April 1985. Local time is shown at the bottom.

sea surface (slicks) alternated with rip bands consisting of 1–2 m high surface waves with white caps.

The highest solitary wave, in the form of a large depression of the sound scattering layers (Fig. 13), was recorded by an echosounder from the drifting R/V *Akademik Alexander Vinogradov* within the Seychelles Archipelago in 1985. This wave was followed by several waves of smaller, but significant amplitude as it should be in a soliton

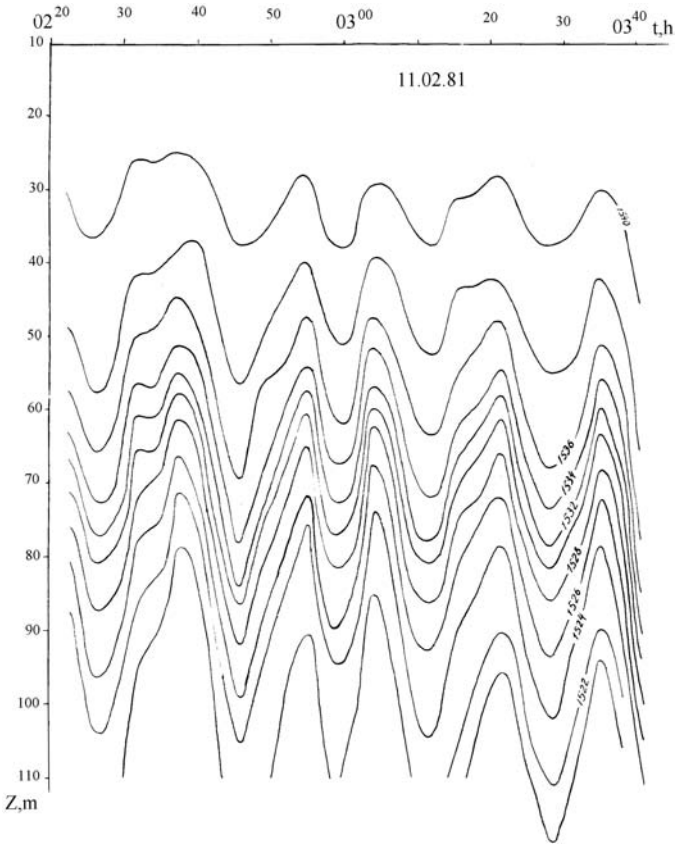

Figure 14. Sound speed isopleths drown by yo-yo CTD data obtained at the eastern slope of the Mascarene Ridge in February 1981. Local time is shown at the top.

train. Many similar trains propagating with speeds of up to 2–2.5 m/s were encountered during the experiments in the Seyshelles Islands. These trains seem to be related to the internal hydraulic jumps generated by tidal currents at the lee side of the underwater shoals and sills common there.

A packet of quasi-periodic IWs of large height (up to 34 m) was encountered during the drift of the R/V *Dmitry Mendeleev* in deep water at the eastern slope of the Mascarene Ridge (Fig. 14). The measurements were carried out using a drifting array of four line sensors spaced horizontally by 100–600 m. The recorded waves propagated eastward from the sill between the Nazareth and Saya-de-Malya banks with a speed of 1.25 m/s, which corresponded to the lowest mode linear wave speed.

In another experiment in 1990 (Konyaev *et al.,* 1995), a packet of intense soliton-like waves was encountered in the same region far (~100 km) from the sill. The packet propagated to the ESE with a speed of about 3 m/s, i.e. much faster than linear waves. (The

measurements were carried out by the towed LS.) The first depression of 90 m, accompanied by a wide ripp band on the sea surface, was followed by a sequence of waves with decreasing amplitude (a rank-ordered sequence typical for solitons) (Konyaev *et al.,* 1995). Such an appearance of internal solitons rather far from the Mascarene Ridge seems to be connected with the nonlinear evolution of the internal tide as it radiates from the sill edge to the open ocean. Large, lowest-mode, soliton-like waves appear at some distance from the sill (about a hundred km) as a result of ray propagation and gradual nonlinear evolution. A similar scenario was observed in the Bay of Biscay (New and Pingree, 1992).

A different scenario takes place for the waves appearing directly at the sill. In this case, the wave generation is connected with the disintegration of a hydraulic jump on the lee side of the underwater sill. Let us consider this scenario using results of the measurements conducted by the R/V *Akademik Nikolay Andreev* in March 17, 1987. These measurements were performed with the help of two (upper and lower) towed gauges, consisting of combinations of 30-m LS's with two point temperature sensors at the ends of each LS. The gauges were towed in the layer including the main part of the upper thermocline. Five tows intersecting the IW trains perpendicularly to the IW fronts were curried out. (The fronts were manifested on the sea surface by bands of rips and slicks elongated mainly from NNE to SSW.)

At the western (lee) side of the sill, we met a sharp disturbance of the thermocline (a hydraulic jump), appearing when the directions of the tidal and steady currents coincide and beginning to propagate eastward against the combined current when the tidal flow starts to slacken. Presumably, the same disturbance, shown in Figure 15, was encountered later at the eastern edge of the sill. This time the disturbance took the form of an undular bore with oscillations of 10–15 m against the overall thermocline depression by 80 m. The wavelengths estimated via radar images of the sea surface were of 0.7 km. The waves propagated to ESE with a speed of 1.5 m/s relative to the water.

Figure 16 shows the ship's trajectory in the time (t)-distance (x) plane and the locations of the wave groups I–VI encountered during the experiment. Wave groups I, II, III, and VI seem to belong to the same train at different stage of its evolution. Estimated wavelengths (l), heights (h) and intrinsic phase speed (c_0) of the wave train are shown in the insert. (Hereafter we define the "wavelength" as the distance between successive oscillations.)

Estimates of the flow velocity above the sill, based on the ship's drift (the right-hand side of Fig. 16), suggest the following development of events. At the moment when the directions of the tidal and westward steady currents coincide, the total flow over the sill with velocities of 1.2–1.5 m/s forms a depression (hydraulic jump) on the lee slope of the sill. (The depression was recorded by the towed LSs.) The velocity C_0 of the wave components, forming this depression, is equal in magnitude and opposite in direction to the total flow, which holds the depression in place. When the tidal flow starts to slacken, the depression begins to propagate eastward against a combined current with increasing velocity $C(t) = C_0 + U_T(t)$, where C_0 is the wave velocity relative to the water, and $U_T(t)$ is the velocity of the combined flow at the time t. Simultaneously, the solitary

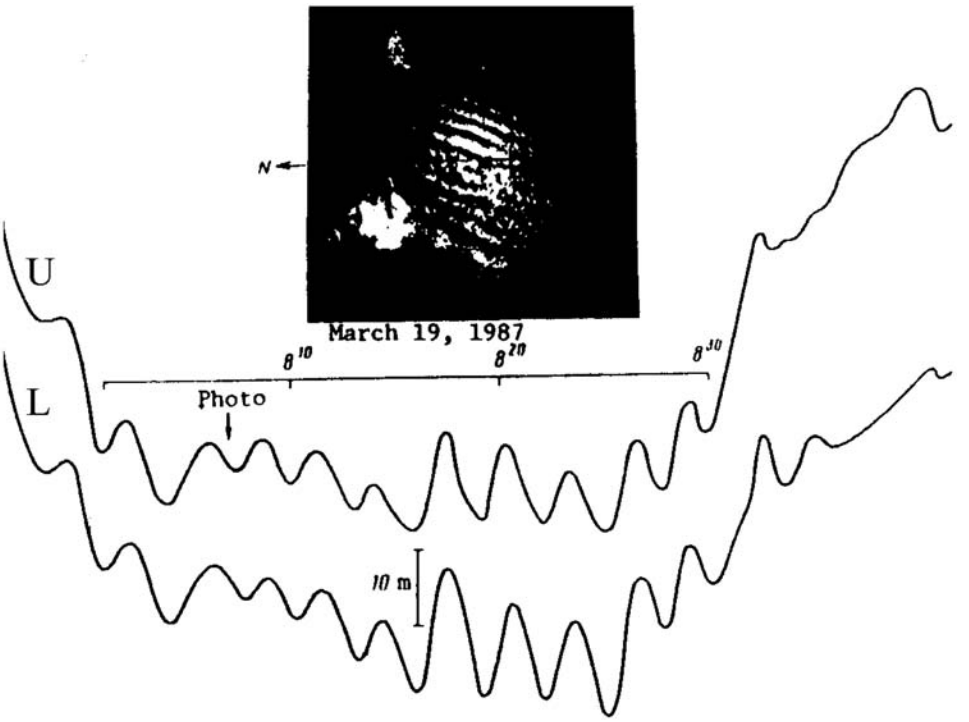

Figure 15. Thermocline displacements according to data from the upper (U) and lower (L) towed gauges (10-m displacement is indicated by bar. Local time is shown above the curves). The record was obtained on the tow track in the WNW direction at the eastern edge of the sill between Nazareth and Saya-de Malya banks. Radar image of the rips related to the IWs is shown in the insert.

depression starts to disintegrate into a train of solitons. (In some sense, the depression itself may be regarded as a collection of solitons, which is manifested in the form of high-frequency oscillations in the trough of the depression.) At first, these are only small oscillations with short wavelengths, but as the solitons disperse (due to the amplitude dispersion), they separate more and more from one another, which is manifested as an increase in the wavelengths and heights of the short-period oscillations in the trough of the depression. Finally, the solitons become almost completely separated from one another, transforming into a quasi-periodic train of high waves—the form of the train, which we met at the end of the two (group VI). The overall depression, uniting the solitons which were previously "stuck together," can no longer be followed at this stage, but the velocity of the waves relative to the water remains the same and close to the velocity of the flow forming the initial depression (the hydraulic jump). The corresponding parameters of groups I, II, III, and VI are shown as functions of time in the insert at the bottom of Figure 16. One can see that the height h and wavelength l of the wave grow with the time t, while

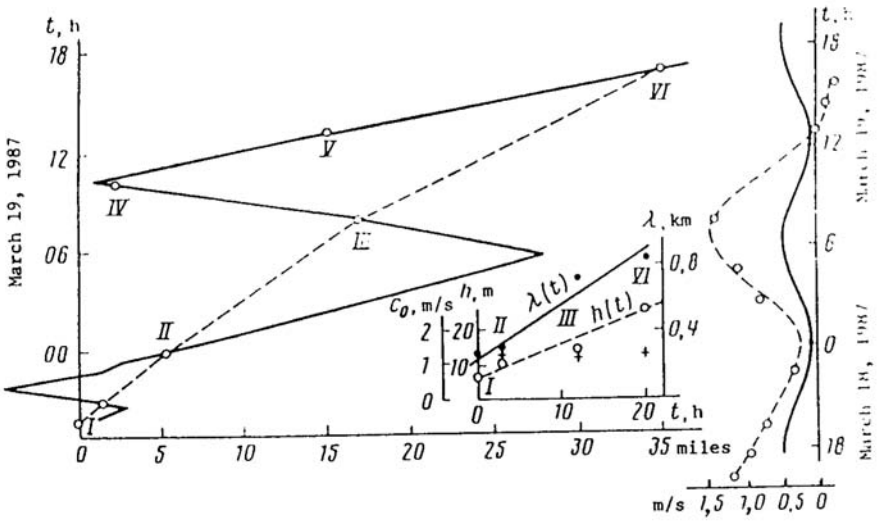

Figure 16. Ship's trajectory (solid straight lines) and trajectories of the wave train (dashed line) in the plane time (t) − distance (x) from the site where the group I was encountered. Right-hand side of figure: estimates of the velocity of the westward flow $U(t)$ (points connected with dashed line) and sea level on the nearby Agalega Islands (solid curve). Insert: wavelengths (dots), heights (circles), and velocity relative to the water (crosses). The Roman numerals indicate the encountered wave groups.

the velocity of the waves relative to the water (C_0) remains practically unchanged. (Equating the rate of increase of the wavelength with the rate of dispersion of the Korteweg-de Vries solitons, we obtain $\Delta C = dl/dt = 1$ cm/s, which corresponds to differences in the amplitudes of the solitons of the order of 1 m).

The average velocity of the soliton train, characterized by the slope of the dashed trajectories in Figure 16, is 0.7 m/s relative to the earth on the section II–III and 1.0 m/s on the section III–VI. If the average drift of the waves by the head-on total flow is added to these values (dashed curve on the right-hand side of Fig. 16), then we obtain velocities of 1.6 and 1.4 m/s, respectively, relative to the water; what agrees quite well with the experimental estimates.

Train IV, encountered 13 h after train I at almost the same location, evidently formed during the next peak of the combined westward current. Estimated propagation velocity of group V relative to the water is so small ($C_0 = 0.4$–0.6 m/s) that it should be carried backward by a stronger head-on flow. This train apparently consists of linear waves left behind by solitons.

A similar scenario of soliton generation was observed here in 1990 (Konyaev *et al.,* 1995), but the estimated speed of propagation of the waves across the sill was about 0.2 m/s, half as much as it was during the observations made in 1987. In 1990 the wave trains did not always propagate to the east but sometimes were retarded and even pushed

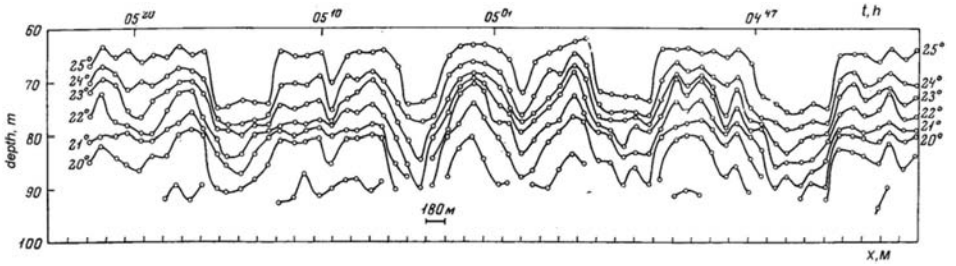

Figure 17. Isopleths of temperature recorded by the towed thermistor chain in the Cape Verde Basin.

back by the combined current. The total propagation time of the waves across the sill was about 24 h. This time was sufficient for the train to disappear into background oscillations. Lack of direct current measurements does not allow one to explain this difference by the different strength of currents in 1987 and 1990 above the sill, although some indirect estimates show that the currents in 1990 were indeed stronger. This seems to be the main reason for the shorter propagation range of the wave trains in 1990 in comparison with the 1987 observations, when the soliton train was encountered at a 50-km distance from the eastern edge of the sill (see Fig. 16). We may suppose also that trains crossing the sill can survive even longer than trains trapped above the sill, where strong mixing occurs.

The observed scenario of the internal soliton generation is rather typical for the underwater sills and has been described in several experimental and theoretical papers. However, there are some distinct features of the waves above and near the Mascarene Ridge. They are as follows: (1) The hydraulic jump is generated on the western side of the sill only. This asymmetry is connected with a strong steady western current crossing the Mascarene Ridge above the sill. It results in an internal hydraulic jump on the lee (western) side of the sill when tidal (semidiurnal) and steady currents coincide, i.e. twice a day. (2) The vertical structure of the hydraulic jump at the sill and of the short-period waves above the sill have strong second mode components. (3) IWs generated by the hydraulic jump do not always cross the sill. (4) The soliton trains appearing at some distance from the sill seem to be connected with the nonlinear evolution of the internal tide as it radiates from the sill edge to the open ocean.

b. Waves intensified by nonuniform currents

Intense IWs occur in some regions of the open oceans far from the bottom topography irregularities above the flat and deep bottom. Intensification of the short-period IWs in these "hot spots" seems to be related mainly to the variations of the background currents and other parameters of the medium in which the waves propagate.

One such "hot spot" apparently related to dynamical processes in the confluence zone between Canary and North-Equatorial currents is located in the Cape Verde Basin. Intense IWs were often encountered in the Basin. Figure 17 shows a record of the waves obtained by a towed thermistor chain from R/V *Sergey Vavilov* in 1967 at about 10N, 31W. Several

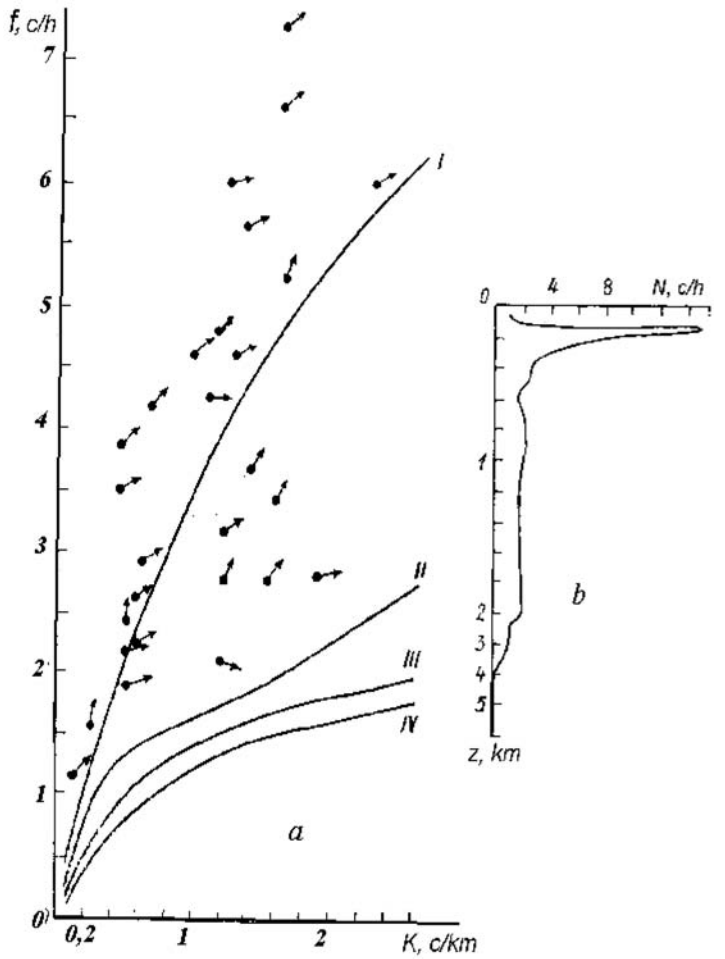

Figure 18. (a) Parameters (wavenumber k, intrinsic frequency ω, direction (arrow) and dispersion relation (for modes *I–IY*) of the waves recorded in the Cape Verde Basin. Upward direction of the arrows is due north. (b) Buoyancy frequency profile.

soliton-like thermocline depressions with amplitude up to 20 m are clearly seen in the record.

In 1984 we carried out the more detailed IW experiment measuring space-time parameters of the short-period waves by means of a drifting array that consisted of four horizontally separated LSs and a chain of five current meters lowered in the thermocline from the drifting ship. The obtained results are shown in Figure 18 together with the buoyancy frequency and corresponding dispersion relation for the waves.

The wave parameters are depicted in a plane $k - \omega$ where k and ω are wavenumber and intrinsic frequency, respectively. The propagation direction is shown by arrows (upward

direction is due north). Nearly all of the waves propagated in the northeastern direction. Most of the $k - \omega$ points in Figure 18a seem to be tended to a straight line tangent to the lowest mode curve at the axis origin. It may be regarded as a hint to the solton nature of the waves since opposite to linear waves, the soliton phase speed does not depend on the frequency and is near to the speed of the low-frequency waves.

Thus, the characteristic profile of the waves recorded in the Cape Verde Basin (Fig. 17), as well as the straight-line dispersion relation of some of the measured waves (Fig. 18a) give evidence about existence of the solitons in the IW field in this region. Generation of the solitons here is hardly connected with the disintegration of the internal tide emanated from the Cape Verde Islands since there were no waves propagating westward (i.e. from the Islands). Other sources such as unstable fronts at the North Equatorial Current edge seem to be more likely.

Anyway, exact causes for occurrence of the intense short-period IWs in the open ocean far from its continental margins above deep and flat bottom remain unclear yet. Generally speaking, short-period internal wave intensification may be connected with certain variations of parameters of the medium in which the waves propagate. The most important variations are mesoscale currents, since their velocity is of the same order as the wave phase speed and the current gradients may be very steep in time and space. A particularly strong effect, leading to wave refraction and a change in wave parameters, is associated with horizontal variations in the currents (Badulin and Shrira, 1993).

Interesting results were obtained during an internal wave experiment which took place in the presence of an anticyclonic eddy at the boundary of the California Current (Sabinin *et al.,* 1990). During March 7–11, 1986 the R/V *Vityaz* performed measurements using a towed array of four line temperature sensors (LS) similar to those described in Section 2b. The configuration of the array is depicted in Figure 19. The measurements of internal wave parameters were made along 12 tracks near the Henderson Seamount, where the background current field was measured by 22 moored current meters (Fig. 20). During March 16–17 1986 the R/V *Dmitriy Mendeleev* performed measurements in the same area with a drifting array of three LS. The mean towing speed was 4 knots and the mean drift speed was 1.5 knots. All sensors covered the core of the upper thermocline (60–110 m).

Intense internal waves with different directions were recorded in the region. Horizontal wavenumber vectors for these waves, estimated by spatio-temporal spectral analysis of the array data, are shown in Figure 20. The background current vectors measured by the moored current meters are also shown in the figure. The southern periphery of the anticyclonic eddy, presumably of topographic origin, can be noticed in the current field, with the southward currents predominant in the eastern part of the study area, and the westward currents predominant in the western part.

The directions of the wave vectors for the wave trains encountered make it possible to distinguish between two regions near the seamount. The first one is a small region at the mount where the wave field rotates clockwise around the mount, which is typical for waves trapped at a local bottom rise. The second one is a broad region of the anticyclonic eddy

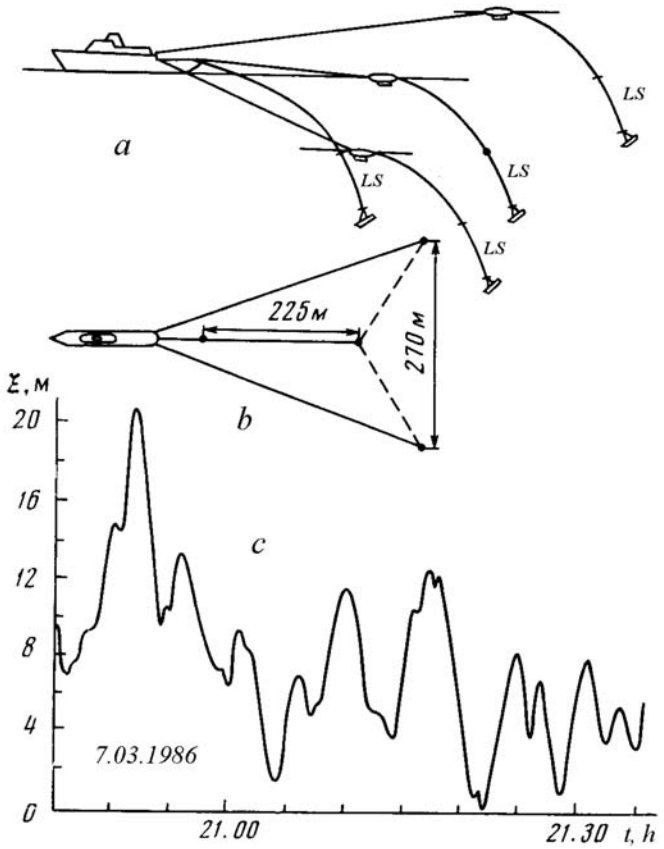

Figure 19. Towed array of LS: (a) overall view; (b) view from above; and (c) a portion of recorded thermocline displacements.

where the wave vectors display a tendency to be nearly perpendicular or opposite to the current. (Apart from the region directly above the seamount, the predominant waves in the eastern part of the test area, where southerly currents dominated, were directed mainly to the northeast, while in the central part of the area, where the current was southwesterly, the waves propagated mainly to the southeast.)

It is natural to look for an explanation for the observed patterns of wave-current interaction using laws governing the conservation of wave action and the changes of wave parameters along ray trajectories (LeBlond and Mysak, 1978). Consider the evolution of wave packets approaching at some angle α to a jet of the steady current $U(y)$ that is directed along the x axis, and varies with y (Fig. 21). Since the current does not vary in time or along Ox, the frequency ω and k_x-component of the wave number remain constant as well, i.e. $\omega = \omega_0 + Uk_x = const$, and $k_x = const$ (ω_0 is the intrinsic frequency). Although the wave number component k_x, which is directed along the current, is

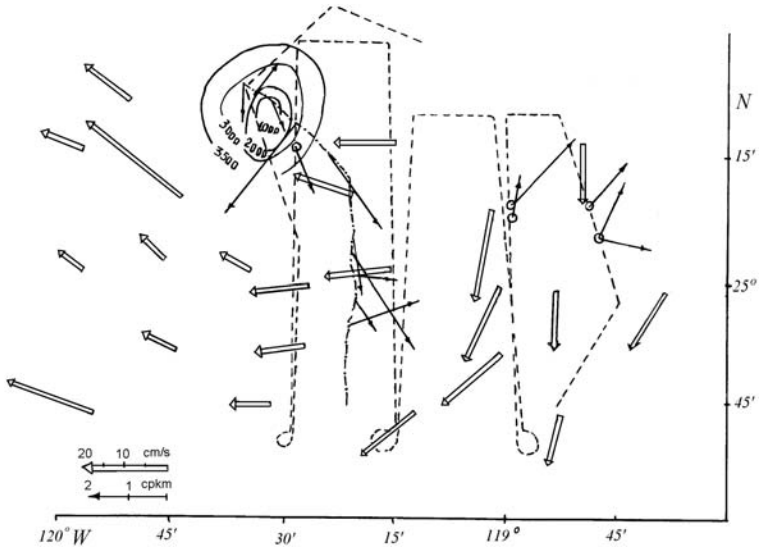

Figure 20. Internal wave vectors (thin arrows) in an anticyclonic eddy. Thick, hollow arrows indicate the low-frequency current field at depth of 75 m. The dotted line indicates the ship track (tacks) during towed array observations, and the dot-dash line indicates the drifting array trajectory. Solid lines indicate isobaths in meters, showing the location of Henderson Seamount.

unchanged, the wave vector $\boldsymbol{k}$ rotates due to current shear in such a way that k_y and the magnitude of the wave number $|k|$ decrease (Fig. 21a). This also leads to a decrease in the intrinsic frequency ω_0, associated with the wave number through the dispersion relation. At the same time, since the wave action $A = E/\omega_0$, is conserved, the decrease in ω_0 leads to the reduction in the energy E of the packet. In addition, typical buoyancy frequency

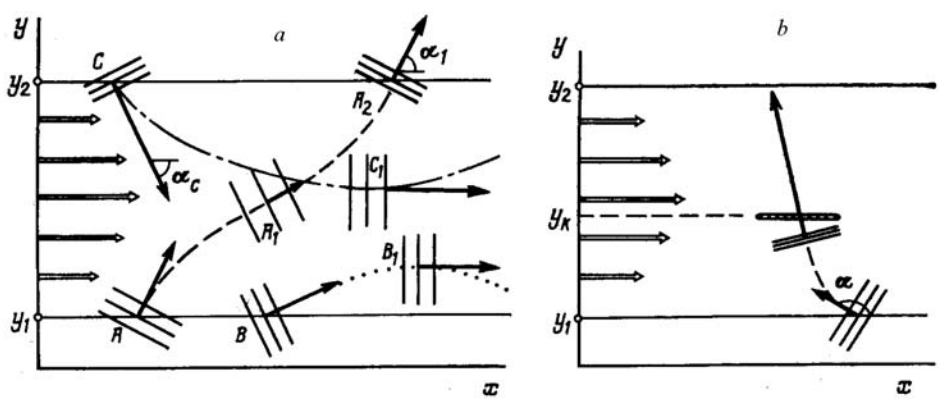

Figure 21. Evolution of wave packets in a horizontally nonuniform current $U(y)$. The k_x-component of the wave number is directed along (a) or opposite (b) to the current.

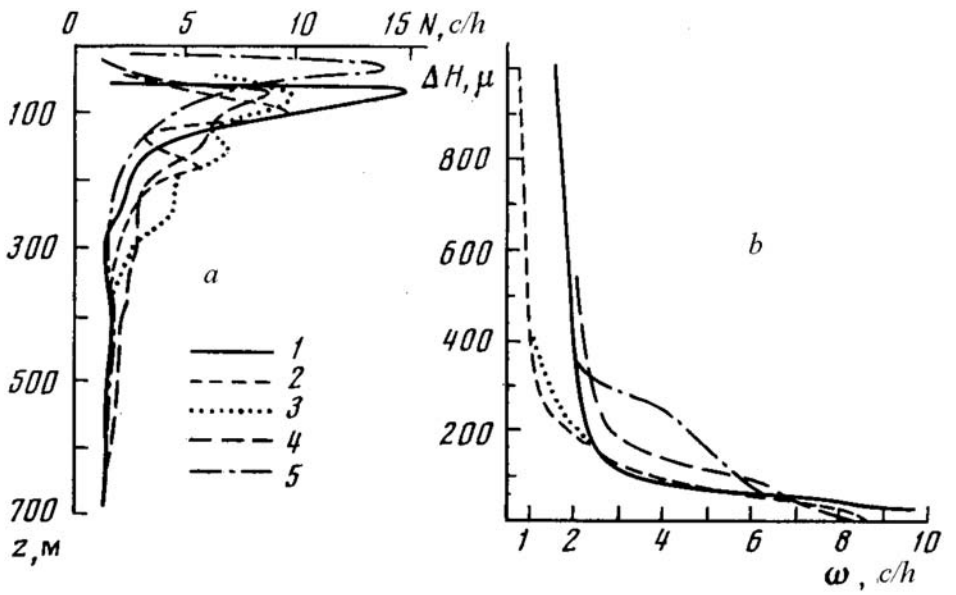

Figure 22. (a) Buoyancy frequency profiles in the test regions: (1) Cape Verde Basin; (2) POLYGON-70 test area; (3) Somali Basin; (4) California Current eddy; (5) POLY1MODE test area; (b) waveguide thickness as a function of the wave frequency for the same five regions.

profiles $N(z)$ are characterized by a maximum in the thermocline (see Fig. 22), which implies a broadening of the waveguide when the frequency decreases (the waveguide for the internal wave with the intrinsic frequency ω_0 is located in a layer where ω_0 is higher than the local buoyancy frequency). Thus, as the packet moves to the jet center, a decreasing amount of energy is distributed over a thickening layer. This leads to a decrease in the amplitude of the oscillations in the pycnocline, and the waves become less pronounced. Upon leaving the jet, all wave parameters are reverted to their initial values (Fig. 21a, packet A. The figure also shows packets B and C, which are reflected by the jet.)

Everything occurs in reverse order for a packet encountering the oncoming current (Fig. 21b). As the thickness of the waveguide decreases, the wave vector deviates more and more from the x axis, and the wave number magnitude, the intrinsic frequency, and the energy of the waves increase. Figure 21b illustrates also the case of complete absorption of a packet in a current. This occurs when the intrinsic frequency tends toward the maximum buoyancy frequency (Badulin and Shrira, 1993). The examples in Figure 21 show that the current jet accentuates the high-frequency components of the wave field traveling against it and suppresses the ones traveling in the same direction.

Let us consider in more detail the case of wave intensification when encountering an oncoming current. For real $N(z)$ profiles encountered in the ocean, there is a frequency ω_c at which the thickness of the waveguide strongly tapers, signifying the transition to the

pycnocline (Fig. 22). When the intrinsic frequency of the waves becomes greater than this value ($\omega_0 > \omega_c$), the energy of the waves, which was previously distributed in a thick waveguide, falls into a steeply tapering waveguide. In this case, the wave components with frequency slightly above the characteristic frequency ω_c and corresponding wavenumber $k(\omega_c)$ become predominant ones in the high-frequency band of the internal wave spectrum distorted by the current.

The first easily observed effect, therefore, is the closeness of the frequency of the dominating short-period waves to the frequency of the steep tapering of the waveguide. The second measurable effect is associated with the directionality of the waves: there should be a propagation component opposite to the direction of the current. Indeed, having $\omega = \omega_0 + U \times k_x = \omega_0 + U \times |k| \times \cos\alpha$ we get: $\cos\alpha = (\omega - \omega_0)/(U \times |k|)$, where α is an angle between the wave vector $\boldsymbol{k}$ and current U direction, ω_0 is the intrinsic frequency, and ω—the frequency measured in fixed coordinates. Then, for the waves influenced by the current we have: $\omega = \omega_c + k(\omega_c) \times U \times \cos\alpha$. One can see, firstly, that the background waves coming into the jet with the initial frequency ω will increase their intrinsic frequencies ω_0 to values $\omega_0 > \omega_c$ (i.e., they will be trapped by a narrow waveguide) only when $\cos\alpha$ is negative. This means that the intensifying waves must have a phase velocity component directed counter to the current. Secondly, the initial frequency of the trapped waves is lower for larger α, with minimum at $\alpha = 180°$, which corresponds to wave propagation in the opposite direction to the current. The following tendency should also be observed: the closer the directions of the incident waves are to the jet normal, the smaller their amplitude and wave length.

All these tendencies can be noticed in Figure 23, which depicts the results of internal wave measurements in various regions of the world ocean. The measurements were made by means of towed and drifting arrays, described above, in the tropical Atlantic (POLYGON-70 test area, and the Cape Verde basin), in the southern part of the Somali Basin (Brekhovsikh *et al.,* 1975), in the Sargasso Sea (POLYMODE test area, Sabinin *et al.,* 1982), and at the California current (Sabinin *et al.,* 1990). The results of the measurements are presented in the form of the wave vectors for various trains depicted in the k-h plane, where h is the wave height. The direction of the wave vectors is shown relative to the current direction (the wave number axis is directed along the current).

Thus, Figure 23 confirms the above theoretical assumptions concerning the main features of intense short-period waves in the current, namely: (a) The angle between the propagation directions of the waves and the current is obtuse ($|\alpha| > 90°$) (a similar connection between the wind direction and the waves has also been observed in the atmosphere (Carter *et al.,* 1984); (b) The smaller the wave number, the larger α and the wave height.

Since mesoscale currents are always present in the ocean, it can be assumed that this mechanism for enhancing of short-period waves propagating at an angle to the current is widespread, and that this mechanism is precisely what explains the observed closeness of

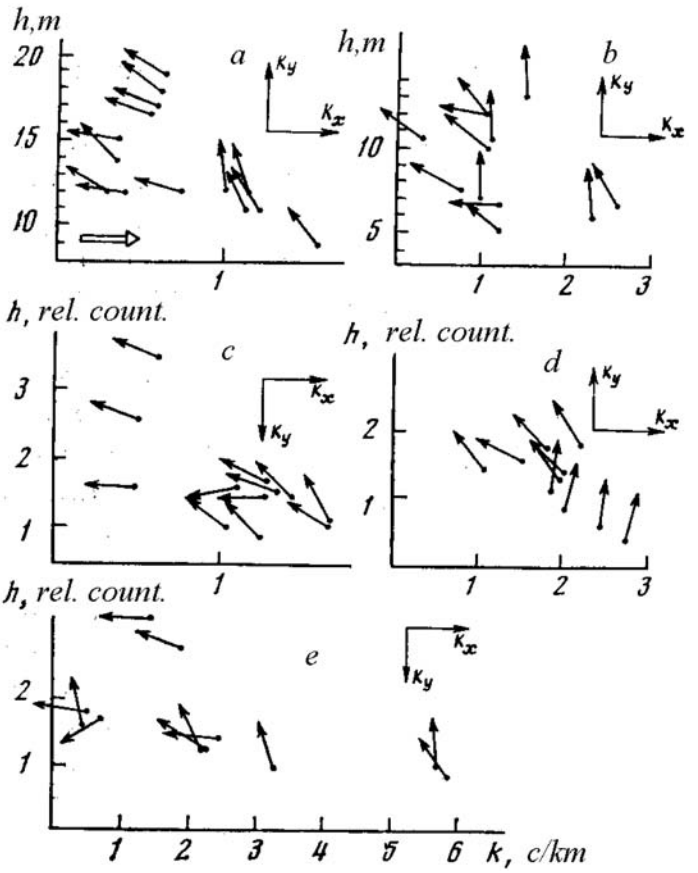

Figure 23. Wave vectors and heights of internal waves measured at (a) POLIGON-70 test area, (b) the California Current, (c) the Cape Verde basin, (d) Somali Basin, (e) the POLYMODE test area. The wave vector indicates the direction of wave propagation relative to the current direction (Ok_x direction). The abscissa of the vector's origin corresponds to the wave number k, the ordinate—to the wave height h.

the wave frequency to the frequency at which the waveguide steeply tapers (Sabinin and Shulepov, 1981).

4. Concluding remarks

Intense short-period IWs in the form of intermittent high-frequency oscillations of the upper thermocline often occur, not only at the shelf edges and oceanic bottom rises, but also in the deep ocean far from bottom topography irregularities. We have investigated these short-period IWs in several representative regions of the world ocean using results of many IW field experiments.

Analysis of the IW field in the Mid-Atlantic Bight and Kamchatka shelf edges, based on results of several experiments, revealed certain features of the IW field in these regions where trains of intense short-period IWs often occur. These regions represent two extreme types of the oceanic continental margins—a broad and relatively flat shelf with not very steep continental slope (the Mid-Atlantic Bight), and a narrow shelf bordering a steep slope with hills at its base (the northwestern Pacific). The existence of internal solitons generated by the disintegration of internal tides and hydraulic jumps is common for both regions, although the spatial structure and the occurrence of the soliton trains on the U.S. Atlantic coast and in the northwestern Pacific are different. Most of the observed trains in the Mid-Atlantic Bight propagate shoreward from the shelf break in the form of soliton packets or solibores and do not occur seaward from the shelf. The soliton trains in the northwestern Pacific at Kamchatka are common not only at the shelf edge but also in deep water where they propagate in various directions. The latter seems to be related to the supercritical steepness and complicated form of the continental slope and the existence of underwater hills. Superposition of the trains radiated from different sources and the interaction of the waves with the meandering Kamchatka Current leads to a very complicated structure of the IW's in time and space. In contrast to the Mid-Atlantic Bight where solibores or dnoidal waves (Apel, 2003) prevail, the intense short-period IWs at Kamchatka often have form of rank-ordered solitons. Also in contrast to the U.S. Atlantic shelf, where the trains occur nearly always (but not always!) twice a day, there is no certain periodicity in the train arrival at Kamchatka. It was established, however, that even in the Mid-Atlantic Bight the semidiurnal periodicity is complicated due to inertial currents. The latter may act not only as another source for the soliton trains but also may modulate the disintegrating internal tides.

Analysis of results obtained at the Seychelles-Mascarene bottom rise, where strong internal tides are generated (Gustafsson, 2001), has shown that internal solitons there are of very large amplitude (up to 100 m and more). Evolution of the wave trains when they propagate from the generation sites at the lee side of the shoals and sills to the deep water was observed by means of towed LS's. At the early stage of evolution, the initial disturbance of the thermocline resembles an undular bore. Later, the short-period oscillations occupying the leading part of the bore start to separate from each other, evolving into a train of solitons with the trailing linear waves. (It seems that the solitons which were previously "stuck together" forming the initial disturbance separate from each other due to amplitude dispersion.) A different scenario, similar to those observed in the Bay of Biscay (New and Pingree, 1992), takes place with the large solitons encountered rather far from the bottom rise. In this case the soliton trains occur in deep water as a result of ray propagation and gradual nonlinear evolution of the internal tide emanated from the Ridge.

Intense short-period IWs encountered far from significant bottom rises are related to variations of the background currents and other parameters of the medium in which the waves propagate. In this context the most important mechanism seem to be the interaction of the high-frequency IWs with horizontally nonhomogeneous currents. The following

features of the intense short-period IWs revealed during the field experiments in several regions of the open ocean may be regarded as evidence for the important role which currents play in wave intensification: (a) a certain dependence of the wave propagation direction on the background current direction, namely, the angle α between the propagation direction of the intense waves and the current is obtuse ($|\alpha| > 90°$); (b) closeness of the intense wave frequency to the frequency at which the waveguide steeply tapers; (c) the smaller the wave number, the larger α and the wave height.

In conclusion, it should be stressed that the role of the inertial waves in the generation of intense short-period IWs in the ocean seems to be underestimated so far. In fact, the nonlinear evolution of strong inertial waves may lead to soliton train generation as happens with strong internal tides. Since the inertial waves sporadically occur everywhere in the world ocean, solitons may also occur everywhere, especially in frontal zones, as has been observed in the confluence zone between the Canary and North-Equatorial currents.

Acknowledgments. The authors wish to express their sincere appreciation to Jim Lynch of the Woods Hole Oceanographic Institution, Rick Chapman of the Applied Physics Laboratory, Johns Hopkins University, and Olga Lavrova of the Space Research Institute, Russian Academy of Sciences, for providing valuable experimental data. Mark Merrifield of the University of Hawaii, Anatoly Nazarov of Andreyev Acoustics Institute, Jim Lynch and Al Plueddeman of the Woods Hole Oceanographic Institution made valuable remarks. The work was partially supported by grant CRDF No. RPO-1340-MO-02

REFERENCES

Alpers, W. 1985. Theory of radar imaging of internal waves. Nature, *314,* 245–247.

Apel, J. R. 2003. A new analytical model for internal solitons in the ocean. J. Phys. Oceanogr., *33,* 2247–2269.

Apel, J. R., M. Badiey, J. Berson *et al.* 1997. An overview of the 1995 SWARM shallow-water internal wave acoustic scattering experiment. IEEE J. Oceanic Eng., *22,* 465–500.

Apel, J. R., H. M. Byrne, J. R. Proni and R. L. Charnell. 1975. Observations of oceanic internal and surface waves from the Earth Resources Technology Satellite. J. Geophys. Res., *80,* 865–881.

Apel, J. R., J. R. Holbrook, A. K. Liu and J. J. Tsai. 1985. The Sulu Sea internal soliton experiment. J. Phys. Oceanogr., *15,* 1625–1651.

Apel, J. R., L. A. Ostrovsky and Y. A. Stepanyants. 1998. Internal solitons in the ocean. Report GOA, No 98-3.

Badulin, S. I. and V. I. Shrira. 1993. On the irreversibility of internal wave dynamics owing to trapping by large-scale flow nonuniformity. J. Fluid Mech., *251,* 21–53.

Brekhovskikh, L. M., K. V. Konyaev, K. D. Sabinin and A. N. Serikov. 1975. Short-period internal waves in the sea. J. Geophys. Res., *80,* 856–864.

Carter, D. A., B. B. Balsley, W. L. Ecklund *et al.* 1984. Tropospheric gravity waves observed by three closely spaced ST radars, *in* Middle Atmosphere Program, URSI/SCOSTEP Workshop on Technical Aspects of MST radar. May 22–25. Handbook for map. 14, 219–228.

Chant, R. J. 2001. Evolution of near-inertial waves during an upwelling event on the New Jersey inner shelf. J. Phys. Oceanogr., *31,* 746–764.

Colosi, J. A., R. C. Beardsley, J. F. Lynch, G. Gawarkiewicz, Chin-Sang Chiu and A. Scotti. 2001. Observations of nonlinear internal waves on the outer New England continental shelf during the summer Shelfbreak Primer study. J. Geophys. Res., *106,* 9587–9601.

Davies, A. M. and J. Xing. 2003. On the interaction between internal tides and wind-induced

near-inertial currents at the shelf edge. J. Geophys. Res., *108*(C3), 3099, doi: 10.1029/2002JC001375, 2003.
Etkin, V. S. *et al.* 1991. Radiophysical aerospace studies of the Ocean. (In Russian). IKI AN SSSR. Preprint PR 1749. 89 pp.
Etkin, V. S., V. A. Razjivin and A. V. Smirnov. 1991. Observation of synoptic eddies in ocean using airborne and ship measurements. Preprint IKI RAS.
Fofonoff, N. P. 1969. Spectral characteristics of internal waves in the ocean. Deep-Sea Res., *16,* 58–71.
Garrett, C. J. R. 2001. What is the "near-inertial" band and why is it different from the rest of the internal wave spectrum. J. Phys. Oceanogr., *31,* 962–971.
Garrett, C. and W. Munk. 1975. Space-time scales of internal waves: A progress report. J. Geophys. Res., *80,* 291–297.
Gasparovic, R. F., J. R. Apel and E. S. Kasischke. 1988. An overview of the SAR internal wave signature experiment. J. Geophys. Res., *93,* 12304–12316.
Gasparovic, R. F. and V. S. Etkin. 1994. An overview of the Joint US/Russia Internal wave Remote Sensing Experiment. IGARSS'94. Digest, 741–743.
Gustafsson, K. E. 2001. Computations of the energy flux to mixing processes via baroclinic wave drag on barotropic tides. Deep-Sea Res. I, *48,* 2283–2295.
Ivanov, V. A. and A. N. Serebryany. 1983. Internal waves on a shallow shelf of free tidal sea. Izv. Acad. Sci. USSR Atmos. Oceanic Phys., *19,* 661–665.
—— 1985. Short-period internal waves in coastal zone of free tidal sea. Izv. Acad. Sci. USSR Atmos. Oceanic Phys., *21,* 648–656.
Jackson, C. R. and J. R. Apel. 2002. An atlas of internal solitary-like waves and their properties. Global Ocean Associates.
Kim, H. R., S. Ahn and K. Kim. 2001. Observations of highly nonlinear internal solitons generated by near-inertial waves off the east coast of Korea. Geophys. Res. Lett., *28,* 3191–3194.
Konyaev, K. V. and K. D. Sabinin. 1992. Waves within the ocean. (In Russian). Gidrometeoizdat, St.-Petersburg, 272 pp.
Konyaev, K. V., K. D. Sabinin and A. N. Serebryany. 1995. Large-amplitude internal waves at the Mascarene Ridge in the Indian Ocean. Deep-Sea Res. I, *42,* 2075–2091.
Kuznetsov, A. S., A. N. Paramonov and Y. A. Stepanyants. 1984. Investigation of solitary internal waves in the tropical zone of West Atlantic. Izv. Acad. Sci. USSR, Atmos. Oceanic Phys., *20,* 975–984.
Lamb, K. G. 1994. Numerical experiments of internal wave generation by strong tidal flow across a finite amplitude bank edge. J. Geoph. Res., *99,* 843–864.
Laurent, L. S., S. Stringer, C. Garrett and D. Perrault-Joncas. 2003. The generation of internal tides at abrupt topography. Deep-Sea Res. I, *50,* 987–1003.
Lavrova, O. Y. and K. D. Sabinin. 1998. Surface manifestations of the deep-ocean internal solitons near Kamchatka. Proceeding of the 4th Pacific Ocean Remote Sensing Conference, (PORSEC'98), Qingdao, China, July 28–31, 1998, 463–465.
LeBlond, P. H. and L. A. Mysak. 1978. Waves in the Ocean, Elsevier, 602 pp.
Legg, S. and A. Adcroft. 2003. Internal wave breaking at concave and convex continental slopes. J. Phys. Oceanogr., *33,* 2225–2246.
Liu, A. K. 1988. Analysis of nonlinear internal waves in the New York Bight. J. Geophys. Res., *93,* 12317–12329.
New, A. L. and R. D. Pingree. 1990. Large-amplitude internal soliton packets in the central Bay of Biscay. Deep-Sea Res., *37A,* 513–524.
—— 1992. Local generation of internal soliton packets in the central Bay of Biscay. Deep-Sea Res., *39A,* 1521–1534.

Sabinin, K. D. 1996. Internal tide in the Kamchatka Current. Oceanology, *36,* 814–818.

—— 1982. High-frequency internal wave spectra in the equatorial Indian Ocean. Oceanology, *22,* 672–676.

—— 1973. Certain features of short-period internal waves in the ocean. Izv. Acad. Sci. USSR Atmos. Oceanic Phys., *9,* 66–74.

Sabinin, K. D., A. A. Nazarov and A. N. Serebryany. 1990. Short period internal waves and currents in the ocean. Izv. Russian Acad. Sci. Atmos. Oceanic Phys., *26,* 621–625.

Sabinin, K. D., A. A. Nazarov and A. N. Serikov. 1982. On the relation between trains of short-period internal waves and thermocline relief in the ocean. Izv. Russian Acad. Sci. Atmos. Oceanic Phys., *18,* 416–425.

—— 1987. Study of high-amplitude internal waves near steep bottom rises. Izv. Acad. Sci. USSR Atmos. Oceanic Phys., *23,* 879–885.

Sabinin, K. D. and V. A. Shulepov. 1981. Towards a model for the internal wave frequency spectrum in the ocean. Izv. Acad. Sci. USSR Atmos. Oceanic Phys., *17,* 67–75.

Serebryany, A. N. 1996. Steepening of the leading and back faces of solitary internal wave depressions and its connection with tidal currents. Dyn. Atmos. Oceans., *23,* 393–402.

—— 2000a. Internal waves on Pacific shelf of Kamchatka (Preliminary results of internal wave field observations), *in* Proceedings of the U.S.-Russia Workshop on Experimental Acoustics, V. I. Talanov, ed., Institute of Applied Physics, Nizhny Novgorod, 116–122.

—— 2000b. Observation of internal waves reflected from the continental slope of Kamchatka. Doclady Russian Acad. Sci., *374,* 1179–1182.

Serebryany, A. N. and H. Pao. 2005. Transition of solitary internal wave through "overturning point" on a shelf. Doclady Russian Acad. Sci. (in press).

Stanton, T. P. and L. A. Ostrovsky. 1998. Observations of highly nonlinear internal solitons over the continental shelf. Geophys. Res. Lett., *25,* 2695–2698.

Vlasenko, V. I., V. A. Ivanov, I. G. Krasin and A. D. Lisichenok. 1998. The generation of intensive short-period internal waves in the frontal zone of a coastal upwelling frontal zone. Phys. Oceanogr., *9,* 155–168.

Vlasenko, V. I., V. T. Paka, N. N. Golenko, K. D. Sabinin and R. Chapman. 1997. Dynamics of baroclinic tides in the USA shelf. Izv. Russian Acad. Sci. Atmos. Oceanic Phys., *33,* 702–714.

Zheng, Q., X. Yan and V. Klemas. 1993. Statistical and dynamical analysis of internal waves on the continental shelf of the Middle Atlantic Bight from space shuttle photographs. J. Geophys. Res., *98,* 8495–8504.

Received: *10 August, 2004;* revised: *21 December, 2004.*